HHS Public Access

Author manuscript

Cell Rep. Author manuscript; available in PMC 2019 February 22.

Published in final edited form as:

Cell Rep. 2019 January 29; 26(5): 1112–1127.e9. doi:10.1016/j.celrep.2019.01.023.

REST and Neural Gene Network Dysregulation in iPSC Models of Alzheimer's Disease

Katharina Meyer[1,5], **Heather M. Feldman**[1,5], **Tao Lu**[1], **Derek Drake**[1], **Elaine T. Lim**[1,2], **King-Hwa Ling**[1,3], **Nicholas A. Bishop**[1], **Ying Pan**[1], **Jinsoo Seo**[4], **Yuan-Ta Lin**[4], **Susan C. Su**[4], **George M. Church**[1,2], **Li-Huei Tsai**[4], and **Bruce A. Yankner**[1,6,*]

[1]Department of Genetics, Harvard Medical School, Boston, MA 02115, USA

[2]Wyss Institute for Biologically Inspired Engineering, Harvard University, Boston, MA 02115, USA

[3]Department of Biomedical Science, Faculty of Medicine and Health Sciences, Universiti Putra Malaysia, 43400 Serdang, Selangor, Malaysia

[4]The Picower Institute for Learning and Memory, Department of Brain and Cognitive Sciences, Massachusetts Institute of Technology, Cambridge, MA 02139, USA

[5]These authors contributed equally

[6]Lead Contact

SUMMARY

The molecular basis of the earliest neuronal changes that lead to Alzheimer's disease (AD) is unclear. Here, we analyze neural cells derived from sporadic AD (SAD), APOE4 gene-edited and control induced pluripotent stem cells (iPSCs). We observe major differences in iPSC-derived neural progenitor (NP) cells and neurons in gene networks related to neuronal differentiation, neurogenesis, and synaptic transmission. The iPSC-derived neural cells from SAD patients exhibit accelerated neural differentiation and reduced progenitor cell renewal. Moreover, a similar phenotype appears in NP cells and cerebral organoids derived from APOE4 iPSCs. Impaired function of the transcriptional repressor REST is strongly implicated in the altered transcriptome and differentiation state. SAD and APOE4 expression result in reduced REST nuclear translocation and chromatin binding, and disruption of the nuclear lamina. Thus, dysregulation of neural gene networks may set in motion the pathologic cascade that leads to AD.

In Brief

*Correspondence: bruce_yankner@hms.harvard.edu.

AUTHOR CONTRIBUTIONS

K.M., H.M.F., T.L., K.-H.L., and Y.P. performed experiments. E.T.L. and G.M.C. generated cerebral organoids. D.D. performed bioinformatics analysis. S.C.S., J.S., and L.-H.T. analyzed electrophysiology. Y.-T.L. generated APOE isogenic lines. N.A.B. generated iPSC lines. K.M., H.M.F., and B.A.Y. wrote the manuscript. B.A.Y. supervised the study.

DECLARATION OF INTERESTS

The authors declare no competing interests.

SUPPLEMENTAL INFORMATION

Supplemental Information includes six figures and seven tables and can be found with this article online at https://doi.org/10.1016/j.celrep.2019.01.023.

Meyer et al. derive neural progenitors, neurons, and cerebral organoids from sporadic Alzheimer's disease (SAD) and APOE4 gene-edited iPSCs. SAD and APOE4 expression alter the neural transcriptome and differentiation in part through loss of function of the transcriptional repressor REST. Thus, neural gene network dysregulation may lead to Alzheimer's disease.

Graphical Abstract

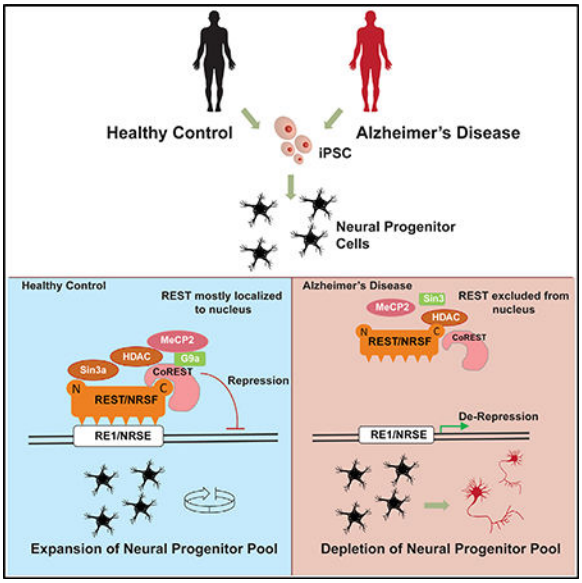

INTRODUCTION

Alzheimer's disease (AD) is the most common neurodegenerative disorder, affecting over 47 million people worldwide (Prince et al., 2016). AD has a long prodromal period that can span decades and is characterized by the accumulation of pathology prior to the onset of memory loss. The molecular basis of these early changes in the brain is unclear. Generation of induced pluripotent stem cells (iPSCs) from patients is an approach to recapitulating the earliest molecular and pathological changes in age-related disorders. Studies of iPSCs derived from AD patients with an *APP* duplication and an SAD patient demonstrated elevated Aβ40 and phosphorylated tau, as well as GSK3β activation, in differentiated neurons (Israel et al., 2012). Increased Aβ42 and tau were also observed in iPSC lines from two patients with the V717I APP mutation (Muratore et al., 2014). In another study, increased accumulation of intracellular Aβ and oxidative stress were observed in one iPSC line from a familial AD patient with an APP mutation and in an iPSC line from a SAD patient (Kondo et al., 2013). In addition, studies of iPSC lines derived from patients with presenilin mutations showed increased Aβ42 levels upon differentiation to neural progenitors or neurons (Sproul et al., 2014; Yagi et al., 2011). Recently, isogenic apolipoprotein E4 (APOE4) lines were reported to show increased levels of phosphorylated tau and Aβ (Knoferle et al., 2014; Lin et al., 2018), as well as increased synapse formation and altered astrocyte and microglial function (Lin et al., 2018). However, a shared phenotype and molecular mechanism among iPSC-derived neural cells from patients with SAD has not been described.

To explore the pathogenesis of SAD, we generated iPSCs from a larger cohort of SAD patients and age-matched controls. Neural progenitor (NP) cells derived from SAD iPSC lines showed a marked increase in the expression of neural differentiation-related genes, leading to premature neuronal differentiation and reduced NP cell renewal. SAD neurons also exhibited accelerated synapse formation and increased electrical excitability. This SAD-related phenotypewasconfirmedinadditionaliPSClinesthatweregenerated in other laboratories. Functional analysis of the transcriptome of SAD NP cells and neurons suggests that upregulated genes are regulated by the transcriptional repressor REST (repressor element 1-silencing transcription factor) (also known as neuronrestrictive silencer factor [NRSF]). REST is a central regulator of neuronal differentiation (Ballas and Mandel, 2005; Chong et al., 1995; Schoenherr and Anderson, 1995) that is induced in the normal aging human brain and reduced in AD (Lu et al., 2014). SAD NP cells showed reduced nuclear REST levels and RESTRE1 site binding. A similar differentiation phenotype and involvement of REST were observed in isogenic neural cells generated from iPSCs that were gene edited to express APOE4, a prevalent genetic AD risk factor. Conversely, gene editing of APOE4 to the neutral allele APOE3 reversed the phenotype. Loss of function of REST in SAD and upon APOE4 expression is due to reduced nuclear translocation and chromatin binding, and is associated with disruption of the nuclear lamina. These findings suggest that REST dysfunction and epigenetic dysregulation emerge in SAD and APOE4 NP cells and persist in differentiated neurons, potentially contributing to the onset of AD.

RESULTS

Reprogramming of Fibroblasts into iPSCs

To obtain NP cells, dermal fibroblast cells from five individuals with SAD and six age-matched, normal controls (NL) were first reprogrammed to iPSCs. Dermal fibroblasts were acquired from the Coriell Cell Repository (Camden, NJ) and the age of biopsy ranged from 60 to 92 years with similar gender representation (Table S1). Reprogramming of iPSCs was achieved through retroviral transduction of *OCT4*, *SOX2*, *KLF4*, and *cMYC* (Park et al., 2008). After isolation of iPSC colonies, stem cell lines underwent a series of quality control measures. High expression of pluripotency markers *NANOG*, *TRA-1–81*, *SOX2*, and *OCT3/4*, as well as *in vitro* and *in vivo* differentiation into all three germ layers and increased alkaline phosphatase enzymatic activity, were confirmed (Figures S1A–S1D; Table S2). All analyzed lines maintained a normal karyotype after reprogramming except SAD1, which showed a balanced translocation between chromosome 3 and chromosome 5 (data not shown). Transcriptional profiling did not show a significant difference in gene expression between the SAD and NL iPSC lines (Figure S1E).

Induction of Genes That Mediate Neurogenesis and Neuronal Differentiation in SAD NP Cells

To generate NP cells, iPSCs were first cultured in suspension as embryoid bodies (EBs) and later plated to form neural rosettes. The neural rosettes were dissociated and grown in the presence of mitogenic factors to become a stable and self-renewing population (Figure 1A). SAD and NL NP cell lines showed similar expression of the NP cell markers Nestin, Musashi, and SOX2 in more than 95% of cells (Figures 1B and 1C). In addition, NP cells

were negative for the pluripotency markers *NANOG*, *OCT3/4*, and *TRA-1–81*, and the glial cell marker *GFAP* (data not shown). DNA fingerprinting of the NP cell and fibroblast cell lines confirmed their identity (Table S2).

Gene expression profiling of NP cells showed robust differences between the SAD and NL lines (Figure 1D; Tables S2 and S3). Gene Ontology enrichment analysis of differentially expressed genes in the SAD lines showed highly enriched categories related to neurogenesis and neuronal differentiation (Figure 1E; Table S3). An overview of genes related to neuronal differentiation is shown in Figure 1F. The most strongly upregulated genes in this category included transcription factors involved in the induction of neurogenesis, such as *ASCL1/MASH1* (8.9-fold), *DLX2* (5.8-fold), and *MEIS1* (5.7-fold), markers of early neuronal differentiation, such as *DCX* (11.4-fold; false discovery rate [FDR] = 0.054), CD24 (8.2-fold), and *STMN2* (13.5-fold), and genes that are involved in axonal targeting such as *EPHB1* (3.7-fold). Thus, by comparing gene expression profiles between SAD and NL NP cell lines from iPSCs, we identified gene enrichment in processes related to neurogenesis and neuronal differentiation.

Early Neuronal Differentiation of SAD NP Cells

A subset of genes upregulated in SAD NP cells was further validated by qRT-PCR. To confirm the reproducibility of these findings, we expanded the qRT-PCR analysis by adding four NL and two SAD NP cell lines generated from iPSCs that were obtained from two different laboratories (Boulting et al., 2011; Israel et al., 2012) (Table S2). In agreement with the transcriptome analysis, expression of the neuronal genes *DCX*, *ASCL1*, *MAPT*, *CD24*, *EPHB1*, and *STMN2* was significantly upregulated in SAD (Figure 2A). Notably, *MAPT*, more commonly known as tau and the primary component of neurofibrillary tangles in AD, was significantly increased in SAD compared to NL. As expected from gene expression profiling, the SAD risk factor gene *APOE* and *CCND2*, a regulator of cell cycle progression and neurogenesis (Kowalczyk et al., 2004), were significantly downregulated in SAD NP cells (Figure 2B). To determine whether the APOE genotype influences the group effect on gene expression, we excluded APOE4 carriers and re-analyzed the data on APOE3/ E3 lines. Importantly, the APOE3/E3 SAD lines consistently showed increased expression of neuronal differentiation genes relative to APOE3/E3 NL lines (Figures S2A and S2B). NP cells were then further analyzed by fluorescence-activated cell sorting (FACS) of the cell surface adhesion protein CD24. CD24 is expressed during developmental and adult neurogenesis and has been used as a marker of early neural lineage specification (Calaora et al., 1996; Pruszak et al., 2009; Yuan et al., 2011). Consistent with the qPCR data, FACS analysis of CD24 showed a significantly increased number of $CD24^{HIGH}$ NP cells in the SAD lines, indicating early neural lineage differentiation (Figures 2C and 2D).

We next assessed neuronal differentiation by immunofluorescence microscopy using nestin and doublecortin (DCX) antibodies. DCX is a microtubule binding protein that is expressed transiently in immature neurons during neurogenesis but is not expressed in mature neurons (Gleeson et al., 1999). Confocal imaging of NP cells showed that most cells expressed the NP cell marker nestin, while a subset of cells expressed DCX (Figures 2E and 2F). DCX-positive cells exhibited neuronal morphology with the elaboration of neuritic processes that

were immunoreactive for the early neuronal marker, β-tubulin III (Figure 2F). Both DCX and the neuronal protein tau were expressed at significantly higher levels in SAD NP cells relative to NL controls (Figures 2E–2G, S2C, and S2D; Table S2). Phosphorylation of tau at Thr231 and Thr205 was not increased (Figure S2D).

The proliferation of SAD NP cells was significantly reduced relative to NL controls, consistent with increased neural differentiation (Figure S2E; Table S2). The decrease in SAD NP cell proliferation was confirmed by decreased incorporation of the S-phase marker EdU (Figure S2F; Table S2), and markedly reduced expression of the NP cell proliferation gene *CCND2* (Figure 2B). Analysis of active β-catenin and cleaved Notch1 by western blotting did not show significant differences in SAD versus NL NP cell lines (Figures S2G and S2H). Thus, changes in Wnt/β-catenin or Notch signaling could not account for the altered differentiation and proliferation of SAD NP cells.

Early Differentiation of SAD NP Cells Is Not Caused by Aβ

Increased accumulation of amyloid-β protein (Aβ) has been implicated in increasing differentiation of NP cells (Lo´pez-Toledano and Shelanski, 2007). Aβ40 and Aβ42 levels were measured in NP cell-conditioned medium by ELISA. Aβ40 levels were significantly increased in the SAD NP cell lines, but Aβ42 levels were below the limits of detection of the ELISA (Figure 2H). To determine whether Aβ plays a role in the differentiation phenotype, three SAD NP cell lines were treated with a BACE1 inhibitor or two different γ-secretase inhibitors, Compound E (CE) and N-[N-(3,5-Difluorophenacetyl)-L-alanyl]-S-phenylglycine t-butyl ester (DAPT), to inhibit Aβ generation. Significant reduction of Aβ40 levels was observed after treatment with the BACE1 inhibitor (50%–59% reduction), and the γ-secretase inhibitors DAPT and CE (65%–75% and 69%–81% reduction, respectively) (Figure 2I). Importantly, expression levels of *DCX*, *ASCL1*, and *CD24* were not significantly decreased by inhibition of Aβ generation (Figure 2J), suggesting that Aβ is unlikely to be related to early neural differentiation in SAD NP cells.

Increased Expression of Neural Gene Networks in SAD Neurons

To explore whether increased expression of neuronal genes is sustained after terminal differentiation of NP cells to neurons, NP cells were differentiated for 6 weeks. More than 75% of all cells exhibited neuronal morphology and positive immunofluorescent labeling of the neuron-specific markers b-tubulin III and MAP2 (Figure S3A). This differentiation protocol yielded two different neuronal subtypes. Glutamatergic neurons, the largest neuronal subpopulation affected in AD, comprised 60%–80% of the neuronal cultures (vesicular glutamate transporter 1 [VGLUT1] positive), while GABAergic (GABA-positive) neurons represent a smaller fraction of 5%–20% (Figure S3B). Unbiased genome-wide expression profiling showed highly significant gene expression differences in SAD compared to NL neurons (Figure S3C; Table S4). Gene Ontology analysis showed that the most significantly upregulated biological processes are related to neuronal maturation, such as nervous system development and synaptic transmission (Figure S3D; Table S4). Specifically, SAD neurons showed upregulation of genes involved in synapse formation, axon guidance, neurotransmitter receptors, and ion channels that play key roles in neurotransmission (Figure S3E). In addition, cell cycle genes were predominantly

downregulated, consistent with accelerated post-mitotic differentiation of SAD neurons. A subset of the SAD neuronal gene expression differences was confirmed in the full cohort of cell lines by qRT-PCR (Figure S4A). Although NP cells represent an earlier stage of neuronal development, SAD NP cells and neurons shared a significant number of upregulated genes related to neural differentiation and function (Figures S4B and S4C).

Accelerated Maturation of SAD Neurons

To determine whether upregulation of neuronal genes accelerates the maturation of SAD neurons, we first assessed synapse formation by quantifying the number of synapsin-1-positive puncta. SAD neurons exhibited significantly increased numbers of synapsin-1-positive puncta relative to NL controls (Figure 3A). These findings were substantiated by patch-clamp electrophysiology. The time course of the appearance of action potentials (APs) was markedly different between SAD and NL neurons (Figure 3B). Generation of APs was detected in the SAD lines by 4.5–7.5 weeks of differentiation, but did not appear in any of the NL lines until 10–12 weeks (Figures 3B and 3C). Even after 10–12 weeks of differentiation, SAD neurons generated significantly more AP spikes than NL controls (Figures 3B and 3C). This difference in the appearance of APs in SAD versus NL neurons was also observed when neurons were co-cultured with astrocytes (Figure 3C). In 10- to 12-week differentiated neurons, the maximum amplitude of APs was calculated from the resting membrane potential (RMP) and threshold potential. SAD neurons showed increased mean maximum AP amplitude relative to NL controls (Figure 3D). Co-culture with rat astrocytes increased the mean maximum AP amplitudes, and there was no significant difference between SAD and NL neurons (Figure 3D). There were also no differences in RMP or threshold potentials between SAD and NL neurons.

We next evaluated sodium and potassium channel dynamics by assessing inward and outward currents in voltage-clamp configuration (Figure 3E). The sodium current amplitude was significantly increased in SAD versus NL neurons, which was largely abolished by astrocyte co-culture at 10–12 weeks of differentiation (Figure 3F). The mean amplitude of potassium outward currents was also significantly higher in SAD compared to NL neurons at every measured time point, and this difference persisted upon astrocyte co-culture (Figure 3G). Taken together, these results suggest that SAD neurons mature more rapidly than NL controls, and maintain increased electrical excitability even after 3 months of differentiation.

We asked whether the accelerated maturation of SAD neurons was accompanied by biochemical changes associated with AD pathology. Phosphorylation of tau is the major biochemical change that underlies neurofibrillary pathology. To assess this change, we analyzed the levels of total and GSK3b-mediated phosphorylated tau by western blot analysis. Significantly increased tau phosphorylation was detected at Thr231 in SAD neurons relative to NL controls but not at Thr205 (Figures S4D and S4E). In addition, levels of Aβ40 trended higher in SAD neurons relative to controls ($p = 0.051$) (Figure S4F). There was no significant difference in Aβ42 (data not shown). These results suggest that the accelerated differentiation of SAD neurons is associated with altered regulation of tau phosphorylation and possibly Aβ generation.

Loss of Function of REST in SAD NP Cells

To identify transcription factors that mediate global gene expression changes in SAD, unbiased transcription factor enrichment analysis was performed using the ENCODE chromatin immunoprecipitation (ChIP) database. This suggested that the transcriptional repressor REST/NRSF and two components of the polycomb repressive complex 2 (PRC2), EZH2 and SUZ12, are the most strongly predicted transcription factors regulating upregulated genes in SAD NP cells and neurons (Figures 4A, 4B, S5A, and S5B). REST has been shown to physically interact with both EZH2 and SUZ12, which can lead to the recruitment of the PRC2 complex (Dietrich et al., 2012; Mozzetta et al., 2014; Tsai et al., 2010). Furthermore, the ChIP ENCODE library showed significant target gene overlap of REST with EZH2 or SUZ12 (Table S5).

Since REST is a transcriptional repressor and was predicted to be a major contributor to gene upregulation in SAD NP cells and neurons, we hypothesized that REST activity was reduced. To address this hypothesis, we first performed REST ChIP, which showed significantly decreased binding of REST to its RE1 binding motif in the target genes *SNAP25*, *SCN3B*, *CALB1*, *DCX*, and *ASCL1* in SAD NP cells relative to controls (Figure 4C; Table S2). Since REST mRNA and protein levels were not significantly different between SAD and NL (Figures S5C–S5E), we assessed nuclear REST by labeling isolated NP cell nuclei with a fluorescent conjugated REST antibody and performing FACS analysis (Figure 4D). FACS analysis showed significantly reduced nuclear REST in SAD NP cells. Furthermore, localization of REST by immunofluorescence showed significantly reduced nuclear and increased cytoplasmic REST in SAD NP cells (Figures 4E and S5F). The reduction in nuclear REST was most pronounced in the subset of DCX-positive cells in multiple SAD NP cell lines (Figures 4F and 4G). In addition, downregulation of REST in normal control NP cells by two different short hairpin RNAs (shRNAs) increased *DCX* expression (Figure 4H). These results suggest that REST function is reduced in SAD NP cells as a result of reduced nuclear translocation and chromatin binding.

Exogenous REST Expression Prevents Early Differentiation of SAD NP Cells

To determine whether overexpression of REST could rescue the differentiation phenotype in SAD NPs, we transduced multiple SAD NP cell lines with lentiviral vectors encoding REST. First, we measured *DCX* gene expression and found significantly decreased *DCX* mRNA expression in SAD NP cells overexpressing REST compared to SAD cells transduced with GFP (Figure 4I). This analysis was expanded to additional genes that are involved in neurogenesis and upregulated in SAD NP cells. REST overexpression reversed gene upregulation of *ASCL1*, *GABRB3*, *MEIS1*, *EPHB1*, *CD24*, *STMN2*, and *SCN2A* (Figure 4J), and increased the expression of genes that are downregulated in SAD NP cells, including the cell proliferation gene CCND2 and the AD risk factor gene *APOE* (Figure 4J). In addition, exogenous REST expression in SAD NP cells significantly reduced the number of DCX-positive neuronal cells (Figures 4K and 4L). These results suggest that REST loss of function contributes to the accelerated differentiation of SAD NP cells.

APOE4 Induces Early Neuronal Differentiation and Dysregulation of REST

The APOE allele E4 is the most significant genetic risk factor for late-onset AD, whereas the prevalent E3 allele (APOE3) is neutral for AD risk (Yu et al., 2014). To explore whether the APOE4 risk allele leads to epigenetic dysregulation and early neuronal differentiation similar to that observed in SAD NP cells, we generated isogenic iPSC lines that differ only in their APOE genotype (Linet al., 2018). By using CRISPR/Cas9 genome editing, a homozygous APOE3 iPSC line from a normal aged donor was edited to APOE4/E4, and an APOE4 homozygous iPSC line derived from a patient with late-onset AD was edited to APOE3/E3. Off-target effects of gene editing were excluded (Lin et al., 2018).

NP cells were derived from the isogenic iPSC lines to explore the effects of APOE genotype on neuronal differentiation. We first determined mRNA expression of genes that were found to be highly upregulated in SAD NP cells. Editing of APOE3 to APOE4 led to dramatically increased expression of the neural differentiation genes *DCX* (~100-fold) and *ASCL1* (~20-fold), as well as the AD-associated neuronal gene *MAPT* (tau, ~3-fold) (Figure 5A). Conversely, editing of APOE4 to APOE3 led to significantly reduced expression levels of *DCX*, *ASCL1*, and *MAPT* (~4- to 5-fold) (Figure 5B). In addition, APOE4 induced a marked increase in the proportion of DCX-positive immature neurons (Figures 5C and 5D) and increased DCX protein expression (Figures 5E and 5F). The APOE4 allele also affected APOE expression, significantly reducing the levels of APOE mRNA and protein (Figures S6A–S6C). Notably, we did not detect significant changes in the levels of activated β-catenin, suggesting that the differentiation changes are unlikely to relate to changes in the canonical Wnt signaling pathway. There was a significant decrease in levels of Notch 1 and the cleaved Notch1 fragment NICD in one isogenic APOE3 line (Figures S6A and S6B). However, this is unlikely to contribute to reduced differentiation of the isogenic APOE3 NP cells, as Notch signaling typically inhibits neural differentiation. These results suggest that APOE4 recapitulates the phenotype of accelerated neuronal differentiation observed in SAD NP cell lines.

We then asked whether altered regulation of REST might contribute to the phenotype of APOE4 NP cells, similar to that observed in SAD NP cells. Confocal immunofluorescence analysis of REST in isogenic NP cells showed that APOE4 significantly reduced nuclear REST levels (Figure 5G), while total REST protein levels were unaltered (Figures S6A and S6B). The reduction in nuclear REST was due to altered REST localization with significantly elevated cytoplasmic REST induced by APOE4. These results suggest that APOE4 leads to reduced nuclear translocation of REST, recapitulating the effects on REST observed in SAD NP cells.

We then asked whether APOE4 might affect epigenetic regulation and neural differentiation at a later stage of neural development. To explore this question, cerebral organoids were generated from isogenic APOE4 and APOE3 iPSC lines (Lancaster et al., 2013). Transcriptome analysis by RNA sequencing (RNAseq) of APOE4 and APOE3 organoids after 46 days of differentiation showed a clear group separation of differentially expressed genes (Figure 6A; Table S6). Gene Ontology annotation and enrichment analysis showed that gene networks associated with nervous system development, synaptic transmission, and neurogenesis were the most significantly upregulated biological processes in APOE4

cerebral organoids (Figure 6B; Table S6). Furthermore, droplet digital PCR confirmed significantly elevated mRNA expression of the neuronal differentiation genes *DCX* and *ASCL1* (Figure 6C), and western blotting showed increased levels of DCX protein in APOE4 compared to APOE3 organoids (Figure 6D). These results suggest that neuronal differentiation might be accelerated in APOE4 organoids. We reasoned that if this were true, it would be reflected in the expression of neural celltype-specific markers. Droplet digital PCR showed a marked elevation in the expression of the mature neuronal markers *NeuN* and *GDAP1L1*, and the synaptic markers *PSD95* and synaptophysin (*SYP*) in APOE4 compared to APOE3 organoids (Figure S6D). The astrocyte marker *GFAP* was expressed at low levels at 46 days and did not differ between APOE3 and APOE4 organoids. The NP cell marker *PAX6* was expressed at a higher level relative to the neuronal markers in APOE3 versus APOE4 organoids, suggesting that NP cells constitute a greater proportion of the cell population in APOE3 organoids (Figure S6D). The stem cell marker *NANOG* was expressed at very low levels in both APOE3 and APOE4 organoids. Comparing the entire profile of differentially expressed genes (DEGs) in APOE4 versus APOE3 organoids with DEGs in SAD versus NL control NP cells and neurons showed highly significant overlaps (Figures S6E and S6F). The most significant overlap of DEGs appeared in APOE4-upregulated genes, which include genes involved in neural differentiation (APOE4 organoid overlap with SAD neurons, p = 2e-36; APOE4 organoid overlap with SAD NP cells, p = 5e-10). Thus, SAD and APOE4 exhibit a common phenotype of early neural differentiation.

APOE4 organoids also showed a significant increase in total tau expression and tau phosphorylated at Ser202, which contributes to neurofibrillary tangle formation in AD (Figure 6D). Thus, early neural differentiation may be accompanied by changes that predispose to AD pathology.

To achieve a greater understanding of altered gene regulation in APOE4 organoids, we performed transcription factor enrichment analysis using the ENCODE database. The transcriptional repressor REST was the most significant predicted regulator of the APOE4-upregulated genes (Figure 6E). Moreover, there was a significant enrichment of REST target genes in the upregulated gene set in APOE4 versus APOE3 organoids (Figure 6F). The REST-interacting genes EZH2 and SUZ12 were the second and third most strongly predicted transcriptional regulators, respectively (Figure 6E). The enrichment of REST, EZH2, and SUZ12 in APOE4-upregulated genes predicts loss of function of these transcriptional repressors, consistent with reduced nuclear REST levels in isogenic APOE4 NP cells. Thus, epigenetic dysregulation through loss of function of REST, and possibly its interactors EZH2 and SUZ12, is a conserved feature of the APOE4 and SAD models.

Disrupted Nuclear Lamina Structure in SAD and APOE4 NP Cells and Neurons

To begin to understand the basis of reduced nuclear translocation of REST in AD, we asked whether the structure of the nuclear envelope might be altered in AD cells. Age-related changes in the nuclear envelope have been reported to impair the import of nuclear proteins (Mertens et al., 2015). To explore the morphology of the nuclear membrane, we performed immunofluorescence microscopy for the nuclear lamina protein lamin B. SAD and APOE4 NP cell lines showed abnormal nuclear lamina morphology characterized by lamin B-

positive invaginations of the nuclear membrane and intranuclear circular structures (Figures 7A and 7C). Both of these abnormal nuclear structures were significantly enriched in SAD and APOE4 NP cells relative to normal and APOE3 NP cells, respectively (Figures 7B and 7D). The mean percent of abnormal cells ranged from 40%–60% of SAD and APOE4 NP cells, which is likely to be an underestimate due to the limited representation of the nucleus upon confocal sectioning. We further differentiated NL and SAD iPSC lines into neurons by induction of neurogenin 2 (NGN2) expression (Zhang et al., 2013). After 14 days in culture, we assessed nuclear lamina morphology by staining for lamin B. Notably, there were significantly increased numbers of abnormal nuclei in SAD neurons compared with NL controls (Figures 7E and 7F). Thus, altered structure of the nuclear envelope/lamina is a common feature of SAD and APOE4 expression that correlates with reduced REST nuclear translocation and chromatin binding.

DISCUSSION

We have identified a shared phenotype of accelerated neural differentiation and epigenetic dysregulation in reprogrammed NP cells and neurons derived from SAD patients and APOE4 gene editing. The ability to model this phenotype *in vitro* might enable the exploration of early steps in the pathogenesis of AD. Network analysis using the ENCODE database implicates the transcriptional repressor REST and the PRC2 core components EZH2 and SUZ12 as the most strongly predicted transcriptional regulators associated with the differentiation phenotype. Since protein interaction and recruitment of PRC2 by REST have been reported (Dietrich et al., 2012; Mozzetta et al., 2014; Tsai et al., 2010), we further validated the contribution of REST to global gene expression changes in SAD and APOE4 NP cells. Nuclear translocation of REST was significantly reduced in both SAD and APOE4 NP cells, together with a major reduction in REST-RE1 site binding in REST target genes in SAD. Furthermore, exogenous expression of REST reversed the accelerated differentiation of SAD NP cells, and conversely, reduction of endogenous REST in normal NP cells mimicked it. These observations suggest that dysregulation of REST may play a central role in the altered gene regulation and accelerated neuronal differentiation associated with SAD and APOE4.

REST plays a key role in the repression of neuronal genes during the early development of the nervous system (Ballas and Mandel, 2005; Chong et al., 1995; Schoenherr and Anderson, 1995) and has been implicated in the regulation of human neurogenesis and neural differentiation (Yang et al., 2012). We have previously demonstrated induction of REST in the aging human brain and a neuroprotective role in neurons (Lu et al., 2014). Furthermore, REST levels decline early in the course of AD in the brain (Lu et al., 2014), in brain-derived exosomes (Winston et al., 2016), and in blood (Ashton et al., 2017). Similarly, PRC2 contributes to neuron specification during differentiation and also represses transcriptional programs that are detrimental to adult neuronal function and survival (Corley and Kroll, 2015; von Schimmelmann et al., 2016). Given the previously described interaction of REST with proteins of the PRC2 complex (Dietrich et al., 2012; Lee et al., 2018), it is likely that the two silencing complexes work in tandem. In addition to recruitment by REST, the enzymatic PRC2 core component EZH2 has been shown to methylate REST, which stabilizes REST when bound to target gene RE1 sites (Lee et al.,

2018). If the methylation of REST by EZH2 is reduced in SAD or in association with APOE4, the REST corepressor will dissociate from RE-1 sites resulting in de-repression of neural differentiation genes, leading to accelerated differentiation and potentially depleting the NP cell pool. In mature neurons, this would lead to de-repression of genes that contribute to AD pathology and promote neuronal cell death (Lu et al., 2014). Thus, impaired function of REST and PRC2 would be expected to have both early and late consequences for the pathogenesis of AD.

The change in cellular localization of REST in SAD and upon expression of APOE4 is consistent with impaired nuclear translocation. However, the magnitude of reduced REST binding to RE1 sites in chromatin is greater than the reduction in nuclear REST levels, suggesting that altered chromatin interactions may play a role in addition to reduced nuclear translocation. This may relate in part to disruption of the nuclear lamina with the appearance of abnormal lamin B-immunoreactive structures that were frequently detected in SAD and APOE4 NP cells and neurons. Similar structural abnormalities in the nuclear lamina have been reported in AD cortical neurons analyzed postmortem (Frost et al., 2016). These changes in nuclear membrane structure and changes in chromatin were associated with increased activity of the tau kinase CDK5 and abnormal tau phosphorylation (Chang et al., 2011; Frost et al., 2014). Our findings suggest that nuclear lamina disruption is an early change in SAD and APOE4 NP cells associated with increased tau expression but not necessarily increased tau phosphorylation, which becomes more pronounced at a later stage. APOE4 might also affect nuclear membrane structure and REST nuclear translocation by altering phospholipid and cholesterol metabolism (Levi et al., 2005; Zhu et al., 2015; Lin et al., 2018). It remains to be determined whether nuclear structural changes affect the function of other transcription factors in AD.

Altered REST function in AD may affect adult hippocampal neurogenesis. Mice in which the REST gene is conditionally deleted in neural stem cells show a transient increase in neurogenesis followed by reduced neurogenesis as the mice age, resulting in fewer hippocampal granule cell neurons (Gao et al., 2011). Similarly, accelerated neural differentiation and reduced progenitor self-renewal associated with reduced REST function in SAD and APOE4 NP cells may lead to early depletion of the NP cell pool. This may, in turn, reduce adult neurogenesis and accelerate the onset of AD by reducing cognitive reserve. It is also possible that increased differentiation of NP cells may have other deleterious effects in the adult brain. For example, it has been reported that overstimulation of NP cell differentiation in adult mice can interfere with memory retrieval, possibly by disruption of neural circuits (Akers et al., 2014).

Our findings raise the possibility that a developmental perturbation, such as depletion of NP cells or altered neural circuit formation, may occur early in life in individuals predisposed to develop SAD. This may not significantly compromise cognitive function in young adults, but may increase the risk of neurodegeneration and cognitive decline in the setting of chronic stressors later in life. In this regard, a functional imaging study showed structural changes in the cortex of infants with an *APOE4* genotype that increases the risk of AD (Dean et al., 2014). Another study that analyzed autobiographical texts written by nuns in

their twenties suggested that some cognitive parameters in young adults may predict later onset of AD (Snowdon et al., 2000).

These observations raise the question of how the classic modulators of AD pathology and disease risk might relate to developmental events in the brain. We noted that many of the genes that are differentially expressed in SAD NP cells are functionally linked to APP and APOE. For example, the developmental protein reelin, which is highly upregulated in APOE4 cerebral organoids, interacts with APP, APOER2, and VLDLR. This interaction affects APP localization and processing and may promote neurite outgrowth (Hoe et al., 2005, 2009). Thrombospondin (*THBS1*) is another ligand for APOER2 and VLDLR that is downregulated in both SAD neurons and APOE4 organoids. It activates the same signaling pathway as reelin and may play a role in promoting neuronal migration in the subventricular zone of the developing brain (Blake et al., 2008). One of the most upregulated genes in SAD neurons is F-spondin (*SPON1*), which binds to APP and facilitates an interaction with APOER2 (Hoe et al., 2005).

There is evidence that APP, presenilins, and APOE, the predominant genetic causes and risk factor for AD, affect neurogenesis and neuronal differentiation. APOE-deficient mice show increased NP cell proliferation in the dentate gyrus at an early age followed by depletion of NP cells later in life (Yang et al., 2011). Furthermore, mouse models of APOE4 expression show increased generation of doublecortin-positive neurons indicative of neurogenesis (Adeosun et al., 2014; Li et al., 2009), similar to the phenotype of SAD and APOE4 NP cells reported here.

Previous studies have demonstrated that Aβ generation is elevated in iPSC-derived neurons with familial Alzheimer's disease (FAD) mutations and in one SAD line (Israel et al., 2012; Kondo et al., 2013; Muratore et al., 2014; Sproul et al., 2014; Yagi et al., 2011). The generation of Aβ was also increased in our SAD NP cell lines. In addition, we observed increased tau phosphorylation in SAD neurons and APOE4 organoids. Importantly, inhibition of Aβ generation with BACE1 and γ-secretase inhibitors did not reverse the accelerated differentiation phenotype of SAD NP cells. Moreover, the differentiation phenotype appeared in NP cells prior to increased tau phosphorylation. Thus, epigenetic dysregulation and altered neural differentiation, mediated in part by REST, may precede the canonical tau and amyloid-related pathology of AD, providing an opportunity for early therapeutic intervention.

STAR+METHODS

CONTACT FOR REAGENT AND RESOURCE SHARING

Requests for resources and reagents should be directed to and will be fulfilled by the Lead Contact, Bruce Yankner (Bruce_Yankner@hms.harvard.edu).

EXPERIMENTAL MODEL AND SUBJECT DETAILS

Induced pluripotent stem cells (iPSCs)—iPSCs were generated from human fibroblasts cells obtained from Coriell using described protocols. Dermal fibroblasts were obtained from the Coriell Cell Repository (Camden, NJ) and reprogrammed through

retroviral transduction of *KLF4*, *SOX2*, *c-MYC*, and *OCT4*. All cases are unrelated except NL6 and SAD5, which are siblings. Additional iPS cell lines were acquired from the Harvard Stem Cell Institute (Cambridge, MA) and from (Israel et al., 2012). Human iPSCs were cultured feeder free with mTeSR1 media (Stem Cell Technologies). APOE genotypes were confirmed by sequencing. Details are listed in Table S1. For all experiments two clonal lines of each isogenic line were used and analyzed.

METHOD DETAILS

iPSC Reprogramming and Culture—iPS cells were generated based on the described protocol with some modifications. pMIG-hKLF4 (Addgene 17227), pMIG-hSOX2 (Addgene 17226), MSCV hc-MYC (Addgene 18119), pMIG-hOCT4 (Addgene 17225), and pMXs-GFP as a positive control were each transfected into Plat-GP cells (Cell Biolabs) using Fugene 6 reagent (Promega) along with pMD2.G (Addgene 12259) containing the VSV-G envelope. All four of the reprogramming factors were linked to GFP with an IRES element. The medium was changed daily until harvest and 0.45 mm filtration at day 4. The retrovirus preparations were ultracentrifuged at 112,000×g for 90 minutes at 4C and resuspended in PBS, pH 7.4. Viral titers were determined by titrating IRES-GFP expression in 293FT cells (Life Technologies). Dermal fibroblasts (5×10^4 cells) were infected with the reprogramming factor viruses at a multiplicity of infection (MOI) of 5 with 4 mg polybrene. Viral transgene induction was verified through expression of IRES-GFP. After four days, the infected fibroblasts were plated on mouse embryonic fibroblasts (iMEFs) inactivated by 10 mg/ml mitomycin C (Sigma-Aldrich) and grown in fibroblast medium (DMEM with 10% FBS, 2 mM L-glutamine, 50 U/ml penicillin, and 50 mg/ml streptomycin) on 0.1% gelatin. After 48 hours, the medium was changed to hESC medium (DMEM/F-12 with 20% knockout serum, 10 ng/ml bFGF (R&D Systems), 1 mM L-glutamine, 100 μM non-essential amino acids, 100 μM 2-mercaptoethanol, 50 U/ml penicillin, and 50 mg/ml streptomycin (all Life Technologies unless noted). Medium was changed daily until iPS colonies formed after 21–30 days. Each colony was isolated and grown on iMEFs as previously described (Park et al., 2008). The hESC medium was changed daily and colonies were passaged every 6–8 days using either manual disruption or collagenase IV enzymatic treatment.

Evaluation of iPS Cells and Pluripotency

Alkaline Phosphatase Assay: The level of alkaline phosphatase activity was evaluated in iPSCs using the Alkaline Phosphatase Detection Kit (Millipore) according to the manufacturer's guidelines. Images of the phosphatase activity were acquired on a brightfield microscope attached to a CCD camera.

Karyotype Analysis: Cytogenetic analysis was performed by Cell Line Genetics (Madison, WI) on twenty G-banded metaphase cells.

Transgene Inactivation: cDNAs for the endogenous and transgenic reprogramming factors were generated from iPS cells. TRIzol-extracted RNA was amplified by RT-PCR in an iQ5 (Bio-Rad) (reverse transcription at 50°C for 30 minutes, denaturation at 95C for 12 min, 60 cycles of amplification (20 s at 95°C, 30 s at 55°C, and 30 s at 68°C) before a final extension of 65°C for 10 minutes. The cDNA product was run on a 2% agarose gel and the correct

product band was extracted using QIAquick Gel Extraction kit (QIAGEN). The product was ethanol precipitated and the final concentration was determined using a NanoDrop 1000 Spectrophotometer. The purified DNA was titrated and used to generate a standard curve for qRT-PCR using QuantiTect SYBR Green RT-PCR kit (QIAGEN). The mRNA concentrations of the reprogramming factors in the iPS cell lines (one clone per case) were determined by comparison with the standard curve following qRT-PCR in an iQ5 (Bio-Rad) using QuantiTect SYBR Green RT-PCR kit (QIAGEN) and a standard cycle of reverse transcription at 50°C for 30 minutes, denaturation at 95°C for 12 min, and then 30 cycles of amplification (20 s at 95°C, 30 s at 55°C, and 30 s at 68°C) before a final extension of 65°C for 10 minutes.

Teratoma Formation: iPS cells growing on 10 cm plates were detached using collagenase and washed with PBS with 0.5% bovine serum albumin (BSA). The pellet was resuspended in 30 μL PBS with 0.5% BSA. The Genome Modification Facility (Harvard University, Cambridge, MA) performed teratoma analysis by injecting 10 μL of iPS cells, containing more than 1×10^6 cells, into the kidney subcapsules of NODSCID mice (three per line). Teratomas appeared after 6–10 weeks and were dissected and fixed in 4% paraformaldehyde (PFA) for 24 hours before being stored in 70% ethanol at 4°C until embedding. The samples were embedded in paraffin, sectioned and stained with hematoxylin and eosin for analysis of cell morphology from each of the three germ layers.

In Vitro Formation of Germ Cell Layers: iPS cells grown on Matrigel hESC-qualified matrix (BD Biosciences) in mTESR1 medium (StemCell Technologies, Inc.) were washed with phosphate buffered saline (PBS) and dissociated with collagenase for 10 minutes at 37°C. After partial dissociation, the colonies were harvested using a cell scraper and pelleted at 200×g for 5 minutes. The colonies were resuspended in Aggrewell medium (StemCell Technologies, Inc.) and transferred to ultra-low attachment plates (Corning) to form embryoid bodies. The medium was changed every 3 days until day 7, when the embryoid bodies were transferred to 0.1% gelatin-coated plates in culture medium (DMEM with 10% fetal bovine serum (FBS), 2 mM L-glutamine, and 1% penicillin/streptomycin (Life Technologies)). The medium was changed every 3 days until day 7, when RNA was isolated in TRIzol. RT-PCR was performed for genes representative of the three germ layers.

DNA Fingerprinting: DNA fingerprinting was performed by Cell Line Genetics (Madison, WI) using the Powerplex 16 kit (Promega). Samples from fibroblasts and NP cells were run in duplicate. The interpreter was blinded to the identity of the samples.

Generation of NP Cells—The protocol for generation of NP cells from iPS cells was adapted from previous reports (Kurosawa, 2007). High density iPS cells growing on iMEF feeders (30–60 cm^2) were primed for neural differentiation two days before passaging by supplementing the hESC medium with 1x N2 supplement (Life Technologies) and the day before passage with 1x N-2 and 1 mM AMPK inhibitor (Calbiochem). The iPSC colonies were detached with dispase, transferred intact using a glass pipette, and washed twice with DMEM/F-12. The colonies were grown in suspension on 10 cm Petri dishes (not treated for tissue culture) to form embryoid bodies (EB) in neural EB (NEB) medium (DMEM/F-12

with 20% knockout serum, 1x N-2 supplement, 1 μM AMPK inhibitor, 1 mM L-glutamine, 100 mM non-essential amino acids, 100 mM 2-mercaptoethanol, 50 U/ml penicillin, and 50 mg/ml streptomycin). Medium was changed every 2–3 days until day 8, when it was changed to neural induction medium (NIM; DMEM/F-12 with 1x N2 supplement, 10 ng/ml bFGF, 1 mM L-glutamine, 100 mM non-essential amino acids, 50 U/ml penicillin, and 50 mg/ml streptomycin). After three more days in suspension, the EBs were plated on 10 cm^2 CELLstart-coated (Life Technologies) tissue culture dishes in NIM, which was changed every 2–3 days until neural rosettes formed (1–4 days). The neural rosettes were manually harvested and transferred intact to plates coated with 0.002% polyornithine (Sigma Aldrich) and 5 mg/ml laminin (Sigma Aldrich). The plates were coated for 2 hours with polyornithine diluted in sterile, distilled water at 37C before washing and coating with 5 mg/ml laminin in calcium/magnesium-free PBS for 2 hours at 37C. The rosettes were grown in NP medium (NPM; Neurobasal medium with 1x B-27 without vitamin A (Life Technologies), 1 mM L-glutamine, 10 ng/ml bFGF, 10 ng/ml leukemia inhibitory factor (LIF, Millipore), 50 U/ml penicillin, and 50 mg/ml streptomycin). Once confluent, the neural rosettes were disrupted and passaged using accutase (StemCell Technologies). The resulting NP cells were plated on polyornithine/laminin-coated dishes in NPM, which was changed every 2–3 days.

Neuronal Differentiation—To induce differentiation, NP cells were plated on dishes coated with polyornithine and laminin (20 μg/ml and 5 μg/ml, respectively) or Matrigel (200 μg/ml) in NPM. After 24 hours, the medium was changed to neuronal medium (NM) containing Neurobasal medium with 1× B-27 (Life Technologies), 1 mM L-glutamine, 50 U/ml penicillin, and 50 mg/ml streptomycin. Half medium changes were performed every 3–4 days. Different surfaces tested included glass coverslips (German, #1.5), plastic coverslips (Thermanox), and plastic tissue culture plates. Some electrophysiological experiments used a protocol in which glass coverslips have hot paraffin drops applied to the surface (3–4 per coverslip). Once the paraffin cooled, the coverslips were coated with polyornithine/laminin on the paraffin surface and NP cells were plated. One day later, the coverslips were inverted over a monolayer of rat astrocytes.

Neuronal Differentiation by NGN2 induction—iPSCs were transduced with a lentiviral vector encoding a doxycycline inducible NGN2 expression cassette and a constitutively expressed YFP fluorescent marker. Transduced iPSCs were then sorted by FACS for YFP expression and maintained under normal culturing conditions. For neuronal induction iPSCs were treated with Rho kinase inhibitors and a single cell solution was obtained by Accutase (StemCell Technologies) treatment. Single cells were plated on Geltrex (Thermo Fisher Scienific) covered 6-well plates and mTeSR1 media was supplemented with 1 μg/ml doxycycline (Sigma Aldrich), cells were then cultured for additional 3 days in mTeSR1 media supplemented with 1 μg/ml doxycycline. After 4 days, neurons were treated with accutase, plated on polyornithine and laminin coated coverslips and cultured using Brainphys media (StemCell Technologies). After 14 days in culture, cells were fixed using 4% PFA in PBS.

Generation of Cerebral Organoids—Cerebral organoids were differentiated using an approach adapted from a previously described protocol (Lancaster et al., 2013). 900,000

iPSCs were seeded into a 96-well ultra-low attachment plate (Thermo Fisher) with 15 ml of mTeSR (StemCell Technologies, Inc.) and 50 μM ROCK inhibitor (Santa Cruz), to obtain embryoid bodies (EBs). The EBs were transferred to 500 μL of neural induction media individually into each well of 24-well ultra-low attachment plates (Thermo Fisher) on Day 6, and another 500ml of neural induction media was added to each well 2 days later. On Day 10, each organoid was placed on parafilm substrate, and 40 μL of Matrigel (Corning #354234) was used for each organoid. Subsequently, we used 1ml of differentiation media with 1% pencillin streptomycin per well every 2–4 days to passage the organoids, and the 24-well plates with the organoids were placed on an orbital shaker at 90 rpm in the incubator. Isogenic lines were derived from parental lines E3 (AG09173) and E4 (AG10788).

Immunofluorescence Microscopy—iPSC colonies were grown on iMEF feeder cells on glass coverslips. NP cells were grown on glass coverslips coated with polyornithine and laminin. For neurons, the NP cells were plated on glass or plastic coverslips at 5×10^4 cells/coverslip and differentiated for 6 weeks before fixation. The cells were washed with Hank's Balanced Salt Solution (HBSS) and fixed with 4% paraformaldehyde (PFA) for 30 minutes at room temperature. Coverslips were washed three times with PBS, incubated with 0.2% Triton X-100 for 20 minutes, and then blocked with 0.02% Triton X-100 and 5% goat serum in PBS for 30 minutes at room temperature. Primary antibodies were diluted in blocking buffer and incubated on coverslips for 1 hour at room temperature followed by 3 washes in PBS and incubation with secondary antibody (1:200 for 1 hour at room temperature; Goat anti-mouse IgG H&L DyLight 488 and Goat anti-rabbit IgG H&L DyLight 594 (Abcam)). The coverslips were incubated 1 hour at room temperature in the dark before washing three times for 5 minutes each with PBS. The coverslip was then inverted on a glass slide with Prolong Gold with DAPI (Life Technologies). For plastic coverslips, the coverslips were covered with and imaged through a larger glass coverslip. The slides were left overnight at room temperature in the dark before image acquisition on an Olympus Fluoview Confocal Laser Scanning Biological Microscope FV1000 (Olympus, USA).

Isogenic APOE lines were cultured on glass coverslips coated with polyornithine and laminin. The cells were washed with Hank's Balanced Salt Solution (HBSS) and fixed with 4% paraformaldehyde (PFA) for 5 minutes at 37C. Coverslips were washed three times with PBS and quenched with 125 mM glycine for 15 minutes. Blocking and permeabilization was performed using 0.3% Triton X-100 and 3% normal donkey serum in PBS for 20 minutes. Primary antibodies were diluted in blocking buffer and incubated on coverslips overnight at 4°C followed by 3 washes in PBS and incubation with secondary antibody (donkey anti-Rabbit Alexa Fluor 488 or donkey anti-mouse Alexa Fluor 647) (Invitrogen) 1:3000 for 1 hour at room temperature. Coverslips were then washed 3 times with PBS and mounted using ProLong Diamond Antifade Mountant (Invitrogen). The slides were left overnight at room temperature in the dark before image acquisition on an Olympus Fluoview Confocal Laser Scanning Biological Microscope FV1000 (Olympus, USA).

For image quantification, at least five randomized fields were imaged per coverslip and cells expressing each marker were counted using the "Multi Wavelength Cell Scoring" application on MetaMorph (v7.7.0.0) software with consistent inclusion criteria for all

coverslips. Synapsin 1 puncta were defined as between 1–8 μm and greater than 1500 times the baseline intensity. For quantification of REST distribution in NP cells, the same laser intensities detector sensitivity and amplification values and offset were used for all micrograph acquisitions. Four random micrographs were acquired from each stained NP cells sample. All acquisition of images for the same experiment were performed at the same time. Raw image files were analyzed using MetaMorph Offline (64-bit) version 7.8.13.0 (Molecular Devices, USA). Multi wavelength cell scoring module with standard algorithm for Adaptive Background Correction system was employed to outline individual NP cell and calculate the averaged and integrated intensities of REST in the nucleus or cytoplasm. Approximate min-max width for DAPI, Alexa Fluor 488 and Alexa Fluor 647 were set at 9–30 μm, 3–30 μm and 3–20 μm, respectively. Thresholding of intensity above local background for DAPI, Alexa Fluor 488 and Alexa Fluor 647 were set at 500, 200 and 100 gray-levels, respectively. The fraction of nuclear REST expression was calculated by dividing the integrated intensity within the nucleus by the integrated intensity of the entire cell. The expression of nuclear and cytosolic REST or the averaged intensity, were calculated by dividing the integrated intensity with the total area of the nucleus or cytoplasm of the same cell.

Quantitative RT-PCR—Primers were designed for 100–250 bp segments spanning exon boundaries highly conserved between alternative transcripts using Ensembl gene mapping information and Primer3 to optimize G/C concentration and melting temperature. Primer sequences are summarized in Table S7. The primer products were verified by agarose gel electrophoresis and a standard curve was established for each primer pair using serial dilution of a titrated RNA sample to account for primer efficiency. RNA was harvested from NP cells or 6-week neuronal cells using either TRIzol reagent or Cells-to-cDNA II kit with DNase treatment. The mRNA was quantified using QuantiTect SYBR Green PCR kit according to the manufacturer's guidelines and run in a one-step RT-PCR cycle in an iQ5 (Bio-Rad) [reverse transcription at 50°C for 30 minutes, denatured at 95°C for 12 minutes, and then subjected to 35 cycles of amplification (20 s at 95°C, 30 s at 55°C, and 30 s at 68°C) before a final extension of 65°C for 10 minutes]. The purity of the PCR products was determined by single peak melting curves. The relative cDNA was quantified using the standard curve established for each primer pair and normalized to *GAPDH* or *β-actin*.

Quantitative droplet digital PCR (ddPCR)—Gene expression in isogenic lines was measured using a TaqMan based assay in the QX200 Droplet Digital PCR System (Bio-Rad). A total of 1 ng RNA was added to each 20 μl reaction of the One-Step RT-ddPCR Advanced Kit for Probes according to the manufacturer's instructions (Bio-Rad). Probe-sets were used in a multiplexed configuration using three targets in one reaction. The plate was then sealed with heat seal foil (Bio-Rad) and droplets were generated using the AutoDG droplet generator (Bio-Rad). The droplet containing plate was then placed in a thermocycler for one-step RT-PCR (reverse transcription at 42°C for 1h, enzyme activation at 95°C for 10 minutes, and then subjected to 40 cycles of amplification (30 s at 95°C and 60 s at 55°C) before enzyme deactivation and a final extension of 98°C for 10 minutes. After thermal cycling the sealed plate was placed in the QX200 Droplet Reader (Bio-Rad) for data acquisition. The resulting data was analyzed using QuantaSoft Software (Bio-Rad).

Fluorescence-activated Cell Sorting (FACS) for CD24—Confluent NP cells were dissociated from 10 cm^2 tissue culture dishes with accutase at 37°C and incubated with 10 U/ml DNase in Neurobasal medium for 10 minutes. The cells were passed through a 40 μm filter, centrifuged, and resuspended in 100 μL NPM with 5 μM EDTA and 0.5% bovine serum albumin (BSA) (about 1×10^6 cells). 20 μL (1 test) of mouse anti-human CD24-FITC (BD Biosciences, 560992) was added per sample and incubated in the dark on ice for 30 minutes. The cells were then washed twice and resuspended in NPM with EDTA and BSA at 2.5×10^5 cells/ml. Cells were stored on ice in the dark until analyzed on a FACSCalibur unit (BD Biosciences) omitting forward and side scatter. Cells incubated without antibody were used as a negative control to adjust settings above autofluorescence.

Western Blotting—For western blot analysis, samples were resuspended in RIPA-DOC lysis buffer (50 mM Tris-Cl, pH 7.2, 150 mM NaCl, 1% Triton X-100, 0.1% SDS, and 1% deoxycholate) with 1× PhosSTOP (Roche) and 1× cOmplete protease inhibitor (Roche) and sonicated for 15 s with a 550 Sonic Dismembrator (Fisher). Protein concentration was measured using DC protein assay kit (Bio-Rad) or BCA protein assay kit (Thermo Scientific) and adjusted to 0.8–1.5 μg/μL in 5x SDS-reducing sample buffer. Equivalent amounts of protein were loaded per lane and resolved by 4%–20% SDS-PAGE. Protein was transferred to PVDF membrane and blocked with 5% nonfat milk in TBS with 0.05% Tween-20 (TBST) for 1 hour at room temperature with shaking. Membranes were cut to allow targeting of multiple size proteins on the same blot and incubated overnight with primary antibody diluted in TBST with 5% bovine serum albumin or 5% nonfat milk and 0.05% sodium azide at 4°C with shaking. The membranes were thoroughly washed with TBST before incubation for 1 hour with peroxidase-conjugated secondary antibody (Jackson ImmunoResearch, 1:2500) in 5% nonfat milk in TBST. After 1 hour, the membranes were washed with TBST before visualization by chemiluminescence (ECL or ECL Prime, GE Healthcare). Intensities of the immunoreactive bands were quantitatively analyzed on a gel documentation system (SynGene). All quantified proteins were normalized to tubulin, GAPDH or b-actin and, if multiple membranes were necessary, also to internal control samples.

Aβ Quantification and Inhibition—Levels of Aβ40 and Aβ42 were quantified in medium conditioned for 5 days by cultures of NP cells or 5–6 week differentiated neurons using ELISA kits according to the manufacturer's instructions (Life Technologies). Two dilutions were made for each sample and Aβ levels were compared to a standard curve generated in each experiment. The Aβ levels were normalized to the total protein levels of the cell lysate in the culture, which was harvested at the same time as the conditioned medium and determined using the DC protein assay kit (Bio-Rad). Aβ production was blocked by treatment with the g-secretase inhibitors DAPT (2 μM) or Compound E (20 nM), or the BACE1 inhibitor IV (0.2 μM) for 4 days. Fresh inhibitors were added every 24 hours. Gene expression was measured using qRT-PCR and normalized to *GAPDH*. Aβ levels in the inhibition experiments were measured using an Aβ40 ELISA kit (Wako) according to the manufacturer's instructions.

Cell Proliferation—NP cells were plated at 5×10^4 cells per well in a 24-well plate and counted on a Z1 Coulter Particle Counter (Beckman Coulter) after 0, 24, and 48 hours. Three replicates were performed, with one well per time point for two experiments and four wells per time point for one experiment. Incorporation of EdU (5-ethynyl-2'-deoxyuridine) was analyzed using Click-IT EdU (Life Technologies) according to the manufacturer's guidelines. NP cells at 50% confluence were incubated with 10 μM EdU for 16 hours. EdU-positive cells were quantified relative to all Hoechst-gated cells. Cells not incubated with EdU were used as a negative control. Two experiments of three replicates each were performed for each line except NDC2.3 (one experiment of three replicates).

Electrophysiology—Neuronal excitability was assessed by whole-cell patch clamping using an Axon Axopatch 200B (Molecular Devices). The operator was blinded to the origin of the culture. The presence of induced APs was determined by measuring voltage in response to current steps ranging from −100 pA to +200 pA. Sodium and potassium channel activity was determined by measuring current in response to voltage steps ranging from −50 mV to +55 mV. The external solution was 130 mM NaCl, 4 mM KCl, 2 mM $CaCl_2$, 1 mM $MgCl_2$, 10 mM HEPES, and 10 mM glucose (pH = 7.4, osmolality = 325 mOsm kg-1). The internal solution was 110 mM potassium gluconate, 20 mM KCl, 2 mM MgATP, 10 mM sodium phosphocreatine, 1 mM EGTA, 0.3 mM GTP-Tris, and 20 mM HEPES (pH = 7.3, osmolality = 320 mOsm kg-1). Pipettes were fire-polished to resistances between 2–4 mOhm and series resistance was compensated 75%. Between 4 and 12 cells were tested per coverslip and the software pClamp10 was used for data analysis. Refer to Table S2 for experimental details.

Isolation of Nuclei and FACS Analysis of REST Levels—Nuclei were isolated from approximately 1×10^6 trypsinized NP cells in 10 mL NF-1 buffer (0.3% Triton X-100, 0.1 M sucrose, 5 mM $MgCl_2$, 1 mM EDTA, 10 mM Tris; pH = 7.5) containing 1× cOmplete protease inhibitor (Roche) and 1 mM PMSF. The collected cells were rocked at 4°C for 30 minutes, then spun down at 1700×g for 10 minutes. The pellets were resuspended in 10 mL NF-1 and rocked 4C for another 60 minutes before being spun down again at 1700×g for 20 minutes. The nuclei were inspected and counted via DAPI staining and resuspended in NF-2 buffer (PBS, 1% BSA, 1× cOmplete protease inhibitor) to a final nuclei concentration of 10^6/ml. To measure REST levels, antibodies against REST protein and isotype-matched control IgGs were pre-conjugated to Allophycocyanin (APC) using lightning-link APC conjugation kit (Innova Biosciences). Approximately 1.5 μl of REST or IgG antibody was added per million cells and incubated at 4°C for 12 hr with gentle rocking in the dark. Labeled nuclei were washed twice by centrifugation with NF-2 buffer, resuspended in 0.3 mL NF-3 buffer (PBS, 1% BSA, 0.1mM $MgCl_2$, 10 μg/mL propodium iodide (PI) and 1× cOmplete protease inhibitor), and filtered through a 0.4 μm cell strainer to remove clumps before performing FACS analysis. The gate was set using the nuclear marker PI to exclude multiple conjugates (high PI labeled) and debris (very low PI = PI-negative) (doublet decrimation). 5000 events were recorded per line. Nonspecific background of the IgG control was subtracted for each cell line. Data was derived from 3–5 replicates per line.

Chromatin Immunoprecipitation—ChIP assays were performed as previously described (Lu et al., 2014). NP cells were cross-linked using 1% formaldehyde at room temperature for 10 minutes. The reaction was stopped by addition of 125 mM glycine and cells were washed twice by centrifugation and resuspension. The cell pellet was then dissolved in SDS lysis buffer (1% SDS, 10 mM EDTA, and 50 mM Tri-HCl, pH 8.1) and the genomic DNA sheared by sonication (Biorupter) at the intensity required to generate 300–1000 bp fragments. The sonicated samples were centrifuged for 10 minutes at 15,000×g at 4°C. The supernatant was diluted 1:10 in ChIP dilution buffer (0.01% SDS, 1.1% Triton X-100, 1.2 mM EDTA, 167 mM NaCl, 16.7 mM Tris-HCl, pH 8.1) and precleared with Protein A Sepharose beads (Life Technologies) before adding REST-antibody conjugation beads. 5% of the sheared DNA was reserved as input control. The sample/beads was incubated for 12 hours with rocking at 4°C and then washed twice with low salt wash buffer and once with high salt wash buffer (0.1% SDS, 1% Triton X-100, 2 mM EDTA, 150 mM NaCl or 500 mM NaCl, 20 mM Tris-HCl, pH 8.1). The beads were washed once with LiCl wash buffer (0.25 M LiCl, 1% NP-40, 1% deoxycholic acid, 1 mM EDTA, 10 mM Tris-HCl, pH 8.1) and twice with TE buffer (1 mM EDTA, 10 mM Tris-HCl, pH 8.1). The beads were then incubated with elution buffer (1% SDS, 0.1 M $NaHCO_3$) for 30 minutes with rocking and vortexed every 10 minutes. The supernatant was transferred to a new tube and 200 mM NaCl was added, followed by de-crosslinking at 65°C for 4 hours. The eluted preparation was treated with RNase A for 10 minutes at room temperature followed by treated with proteinase K and 10 mM EDTA for 1 hour at 55°C. DNA was isolated using the QIAGEN PCR purification kit and PCR was run using primers directed to the RE1 binding site of DCX or GABRB3.

Gene Manipulation of REST—The REST gene was overexpessed in NP cells by lentiviral transduction of a construct encoding the ubiquitin C promoter and REST or GFP as a control, as previously described (Lu et al., 2014). *DCX* gene expression was measured 1 and 2 weeks after infection, while quantification of all other genes and was performed after 1 week. Cells were labeled for nestin, DCX, and DAPI according to the above procedure with secondary antibodies of α-mouse IgG Alexafluor-647 (A21235, Life Technologies) and α-rabbit DyLight 594 (Abcam). DCX-positive cells were quantified 1 week after infection using MetaMorph (v7.7.0.0) software with consistent inclusion criteria. Data is the mean from four different experiments with greater than 3 fields scored per experiment. REST knockdown was performed using either of two distinct shRNAs by lentiviral transduction as previously described (Lu et al., 2014). An shRNA with a scrambled sequence was used as a control. *DCX* expression levels were measured 1 week after infection. REST overexpression was confirmed by qRT-PCR and REST knockdown by western blotting.

RNA library preparation and sequencing—For each biological replicate, 15 cerebral organoids were pooled and pelleted at 1000 g for 1 minute. The supernatant was removed and the organoids were washed twice in D-PBS without calcium and magnesium, before homogenization in lysis buffer and RNA extraction using the PureLink RNA Mini Kit (Thermo Fisher). Purified RNA was treated with DNase I (Thermo Fisher) and sent on dry ice to Macrogen for rRNA-depletion using TruSeq Stranded RNA with Ribo-Zero (Human) and paired-end 101bp sequencing with at least 30 million reads per sample.

RNA sequencing read alignment and quantification of gene expression—

Organoids: Reads were aligned to GRCh38 with Ensembl GRCh38.92 gene models using STAR version 2.5.4a with options --alignSJDBoverhangMin 1 --alignSJoverhangMin 8 --outFilterMultimapNmax 20 --outFilterType BySJout --alignIntronMin 20 --alignIntronMax 5000000 --alignMatesGapMax 5000000. Expression levels of genes were quantified as gene counts using STAR version 2.5.4a with option --twopassMode Basic.

Gene expression sample groups

Neurons: There were 2 groups, SAD and Normal, and each group had 5 biological replicates.

NP cells: There were 2 groups, SAD and Normal, and each group had 5 biological replicates.

IPSCs: There were 2 groups, SAD and Normal. SAD had 5 biological replicates and Normal had 6 biological replicates. One SAD sample, iPSC_SAD1.1, had degraded RNA and was removed from analysis leaving SAD with 4 biological replicates.

Organoids: There were 2 groups, E4 and E3 ISO, and each group had 3 biological replicates.

Gene expression normalization

Neurons, NP Cells, IPSCs: Gene expression profiling was performed using Affymetrix U133 Plus 2.0 arrays. Each dataset was analyzed separately and similarly. We utilized a chip description file to reorganize probes to Ensembl gene ids (version 22.0.0 [Dai et al., 2005]). This converted 54675 probe sets to 20118 Ensembl genes. Gene ids without annotation were then removed leaving 20027 expressed genes for analysis. Raw intensity values for each gene were transformed using robust multi-array average function (rma) from the affy R package with arguments fast = FALSE, normalize = TRUE, background = TRUE. These normalized gene expression values were used to visualize gene expression and for differential expression analysis.

Organoids: Gene counts were input to edgeR. Genes were deemed expressed if > = 3 samples had > = 1 counts per million (CPM). Genes not satisfying these criteria were removed keeping the original library sizes. Of 58395 annotated genes this filtering retained 16581 expressed genes. Counts were then normalized using the TMM method in edgeR. Finally, log(CPM) values were calculated for analyses other than differential expression. These normalized gene expression values were used to visualize gene expression.

To visualize DEGs in heatmaps normalized gene expression values were transformed to a z-score per gene and thresholded to [−3, 3].

Differential expression analysis

Neurons, NP Cells, IPSCs: Each dataset was analyzed separately and similarly. Differential expression analysis between the SAD and normal (NL) groups was performed using linear

regression models in limma in R. lmFit used arguments method = “robust” and maxit = 1000. eBayes used default arguments. Genes were considered differentially expressed if FDR < 0.05 and absolute value(fold change) > = 1.2.

Organoids: Differential expression analysis of APOE4 CTR versus APOE3 ISO was performed for expressed genes using edgeR (estimateDisp, glmFit, and glmLRT with default arguments) in R. Genes were considered differentially expressed if FDR < 0.05.

Gene sets and gene set enrichment analysis—Gene annotation and gene sets used for functional gene classification into biological process (BP), molecular function (MF), and cellular component (CC) were from the GRCh38.p12 database downloaded from Ensembl Biomart on March 4, 2018.

ENCODE ChIP-seq transcription factor target gene sets were from the ENCODE_TF_ChIP-seq_2015 database downloaded from http://amp.pharm.mssm.edu/Enrichr/ on March 8, 2018 (Chen et al., 2013).

To calculate the statistics for overlap of REST, EZH2, and SUZ12 target genes using the ENCODE ChIP-seq database we used the cell line with the most significant overlap with the upregulated genes for NPCs or organoids and used the SuperExactTest R package.

REST target genes. The REST RE1 motif position-specific weight matrix MA0138.2 was obtained from JASPAR. FIMO was used with the Homo sapiens genome sequence GRCh38 to predict REST binding sites. A gene was defined to be a REST target if it had a RE1 motif with motif pvalue < 1e-7 that was ± 10kb from the transcription start site of any transcript of the gene in the Ensembl GRCh38.86 gene models. This procedure identified 2632 REST target genes before filtering for expressed genes in each dataset during gene set enrichment analysis.

For gene set enrichment analysis of DEGs, we only retained genes in each gene set that were expressed in that differential expression analysis. Gene set enrichment analysis was performed separately for upregulated genes versus not upregulated genes, downregulated genes versus not downregulated genes, and differentially regulated genes versus not differentially regulated genes. For Gene Ontology gene sets, gene set enrichment was determined using the TopGO R package using the classic algorithm and Fisher’s statistic. Gene set enrichment for other gene sets was performed using the hypergeometric distribution (one-tailed). Gene sets with < 5 genes after filtering for expressed genes were removed before the gene set enrichment false discovery rates were calculated using the R function p.adjust with argument method = “fdr.”

QUANTIFICATION AND STATISTICAL ANALYSIS

Statistical Analysis—Statistical analysis was performed using R, Graphpad Prism, and Excel. Statistical analysis details are described in the figure legends. To determine if datasets show a normal distribution, the Shapiro-Wilk test was used. P values less than 0.05 were considered statistically significant.

DATA AND SOFTWARE AVAILABILITY

Gene expression data are available in the Gene Expression Omnibus under accession number GEO: GSE117589.

Supplementary Material

Refer to Web version on PubMed Central for supplementary material.

ACKNOWLEDGMENTS

We thank Lawrence Goldstein and Kevin Eggan for providing iPSC lines, George Daley for providing reprogramming vectors, and Laurence Daheron, Cathy McGillivray, Zhenjuan Wang, Sukhee Cho, and Jun Wang for assistance. This work was supported by NIH grants DP1OD006849, R01AG046174, and RF1AG048056 to B.A.Y., R01AG046174 and RF1AG048029 to L.-H.T., and RM1HG008525 to G.M.C.; grants from the Paul F. Glenn Foundation for Medical Research to B.A.Y. and L.-H.T.; a grant from Fidelity Biosciences Research Initiative to B.A.Y.; and grants from the Robert A. and Renee E. Belfer Family Foundation and Cure Alzheimer's Fund to L.-H.T. K.M. was supported by DFG Fellowship ME 4810/1-1, and K.-H.L. was a recipient of an IBRO/ISN Research Fellowship.

REFERENCES

Adeosun SO, Hou X, Zheng B, Stockmeier C, Ou X, Paul I, Mosley T, Weisgraber K, and Wang JM (2014). Cognitive deficits and disruption of neurogenesis in a mouse model of apolipoprotein E4 domain interaction. J. Biol. Chem 289, 2946–2959. [PubMed: 24324264]

Akers KG, Martinez-Canabal A, Restivo L, Yiu AP, De Cristofaro A, Hsiang H-L, Wheeler AL, Guskjolen A, Niibori Y, Shoji, et al. (2014). Hippocampal neurogenesis regulates forgetting during adulthood and infancy.Science 344, 598–602. [PubMed: 24812394]

Alexa A, and Rahnenfuhrer J (2016). topGO: Enrichment Analysis for Gene Ontology. R package, version 2.30.1 (Bioconductor).

Ashton NJ, Hye A, Leckey CA, Jones AR, Gardner A, Elliott C, Wetherell JL, Lenze EJ, Killick R, and Marchant NL (2017). Plasma REST: a novel candidate biomarker of Alzheimer's disease is modified by psychological intervention in an at-risk population. Transl. Psychiatry 7, e1148. [PubMed: 28585932]

Ballas N, and Mandel G (2005). The many faces of REST oversee epigenetic programming of neuronal genes. Curr. Opin. Neurobiol 15, 500–506. [PubMed: 16150588]

Blake SM, Strasser V, Andrade N, Duit S, Hofbauer R, Schneider WJ, and Nimpf J (2008). Thrombospondin-1 binds to ApoER2 and VLDL receptor and functions in postnatal neuronal migration. EMBO J. 27, 3069–3080. [PubMed: 18946489]

Boulting GL, Kiskinis E, Croft GF, Amoroso MW, Oakley DH, Wainger BJ, Williams DJ, Kahler DJ, Yamaki M, Davidow L, et al. (2011). A functionally characterized test set of human induced pluripotent stem cells. Nat.Biotechnol 29, 279–286. [PubMed: 21293464]

Calaora V, Chazal G, Nielsen PJ, Rougon G, and Moreau H (1996). mCD24 expression in the developing mouse brain and in zones of secondary neurogenesis in the adult. Neuroscience 73, 581–594. [PubMed: 8783272]

Chang K-H, Multani PS, Sun K-H, Vincent F, de Pablo Y, Ghosh S, Gupta R, Lee H-P, Lee HG, Smith MA, and Shah K (2011). Nuclear envelope dispersion triggered by deregulated Cdk5 precedes neuronal death.Mol. Biol. Cell 22, 1452–1462. [PubMed: 21389115]

Chen EY, Tan CM, Kou Y, Duan Q, Wang Z, Meirelles GV, Clark NR, and Ma'ayan A (2013). Enrichr: interactive and collaborative HTML5 gene list enrichment analysis tool. BMC Bioinformatics 14, 128. [PubMed: 23586463]

Chong JA, Tapia-Ramírez, Kim S, Toledo-Aral JJ, Zheng Y, Boutros MC, Altshuller YM, Frohman MA, Kraner SD, and Mandel G (1995). REST: a mammalian silencer protein that restricts sodium channel gene expression to neurons. Cell 80, 949–957. [PubMed: 7697725]

Corley M, and Kroll KL (2015). The roles and regulation of Polycomb complexes in neural development. Cell Tissue Res. 359, 65–85. [PubMed: 25367430]

Dai M, Wang P, Boyd AD, Kostov G, Athey B, Jones EG, Bunney WE, Myers RM, Speed TP, Akil H, et al. (2005). Evolving gene/transcript definitions significantly alter the interpretation of GeneChip data. Nucleic Acids Res. 33, e175–e175. [PubMed: 16284200]

Dean DC, 3rd, Jerskey BA, Chen K, Protas H, Thiyyagura P, Roontiva A, O'Muircheartaigh J, Dirks H, Waskiewicz N, Lehman K, et al. (2014). Brain differences in infants at differential genetic risk for late-onset Alzheimer disease: a cross-sectional imaging study. JAMA Neurol. 71, 11–22. [PubMed: 24276092]

Dietrich N, Lerdrup M, Landt E, Agrawal-Singh S, Bak M, Tommerup N, Rappsilber J, So¨dersten E, and Hansen K (2012). REST-mediated recruitment of polycomb repressor complexes in mammalian cells. PLoS Genet. 8, e1002494. [PubMed: 22396653]

Frost B, Hemberg M, Lewis J, and Feany MB (2014). Tau promotes neurodegeneration through global chromatin relaxation. Nat. Neurosci 17, 357–366. [PubMed: 24464041]

Frost B, Bardai FH, and Feany MB (2016). Lamin dysfunction mediates neurodegeneration in tauopathies. Curr. Biol 26, 129–136. [PubMed: 26725200]

Gao Z, Ure K, Ding P, Nashaat M, Yuan L, Ma J, Henner RE, and Hsieh J (2011). The master regulator REST/NRSF controls adult neurogenesis by restraining the neurogenic program in quiescent cells. J. Neurosci 31, 9772–9786. [PubMed: 21715642]

Gleeson JG, Lin PT, Flanagan LA, and Walsh CA (1999). Doublecortin is a microtubule-associated protein and is expressed widely by migrating neurons. Neuron 23, 257–271. [PubMed: 10399933]

Hoe H-S, Wessner D, Beffert U, Becker AG, Matsuoka Y, and Rebeck GW (2005). F-spondin interaction with the apolipoprotein E receptor ApoEr2 affects processing of amyloid precursor protein. Mol. Cell. Biol 25, 9259–9268. [PubMed: 16227578]

Hoe H-S, Lee KJ, Carney RSE, Lee J, Markova A, Lee J-Y, Howell BW, Hyman BT, Pak DTS, Bu G, and Rebeck GW (2009). Interaction of reelin with amyloid precursor protein promotes neurite outgrowth. J. Neurosci 29, 7459–7473. [PubMed: 19515914]

Israel MA, Yuan SH, Bardy C, Reyna SMS, Mu Y, Herrera C, Hefferan MP, Van Gorp S, Nazor KL, Boscolo FS, et al. (2012). Probing sporadic and familial Alzheimer's disease using induced pluripotent stem cells.Nature 482, 216–220. [PubMed: 22278060]

Knoferle J, Yoon SY, Walker D, Leung L, Gillespie AK, Tong LM, Bien-Ly N, and Huang Y (2014). Apolipoprotein E4 produced in GABAergic interneurons causes learning and memory deficits in mice. J. Neurosci 34, 14069–14078. [PubMed: 25319703]

Kondo T, Asai M, Tsukita K, Kutoku Y, Ohsawa Y, Sunada Y, Imamura K, Egawa N, Yahata N, Okita K, et al. (2013). Modeling Alzheimer's disease with iPSCs reveals stress phenotypes associated with intracellular Aβ and differential drug responsiveness. Cell Stem Cell 12, 487–496. [PubMed: 23434393]

Kowalczyk A, Filipkowski RK, Rylski M, Wilczynski GM, Konopacki FA, Jaworski J, Ciemerych MA, Sicinski P, and Kaczmarek L (2004). The critical role of cyclin D2 in adult neurogenesis. J. Cell Biol 167, 209–213. [PubMed: 15504908]

Kurosawa H (2007). Methods for inducing embryoid body formation: in vitro differentiation system of embryonic stem cells. J. Biosci. Bioeng 103, 389–398. [PubMed: 17609152]

Lancaster MA, Renner M, Martin C-A, Wenzel D, Bicknell LS, Hurles ME, Homfray T, Penninger JM, Jackson AP, and Knoblich JA (2013). Cerebral organoids model human brain development and microcephaly. Nature 501, 373–379. [PubMed: 23995685]

Lee SW, Oh YM, Lu Y-L, Kim WK, and Yoo AS (2018). MicroRNAs overcome cell fate barrier by reducing EZH2-controlled REST stability during neuronal conversion of human adult fibroblasts. Dev. Cell 46, 73–84.e7. [PubMed: 29974865]

Levi O, Lu€tjohann D, Devir A, von Bergmann K, Hartmann T, and Michaelson DM (2005). Regulation of hippocampal cholesterol metabolism by apoE and environmental stimulation. J. Neurochem 95, 987–997. [PubMed: 16190879]

Li G, Bien-Ly N, Andrews-Zwilling Y, Xu Q, Bernardo A, Ring K, Halabisky B, Deng C, Mahley RW, and Huang Y (2009). GABAergic interneuron dysfunction impairs hippocampal neurogenesis in adult apolipoprotein E4 knockin mice. Cell Stem Cell 5, 634–645. [PubMed: 19951691]

Lin Y-T, Seo J, Gao F, Feldman HM, Wen H-L, Penney J, Cam HP, Gjoneska E, Raja WK, Cheng J, et al. (2018). APOE4 causes widespread molecular and cellular alterations associated with Alzheimer's disease phenotypes in human iPSC-derived brain cell types. Neuron 98, 1294. [PubMed: 29953873]

Lo´pez-Toledano MA, and Shelanski ML (2007). Increased neurogenesis in young transgenic mice overexpressing human APP(Sw, Ind). J. Alzheimers Dis 12, 229–240. [PubMed: 18057556]

Lu T, Aron L, Zullo J, Pan Y, Kim H, Chen Y, Yang T-H, Kim H-M, Drake D, Liu XS, et al. (2014). REST and stress resistance in ageing and Alzheimer's disease. Nature 507, 448–454. [PubMed: 24670762]

Mertens J, Paquola ACM, Ku M, Hatch E, Bo¨hnke L, Ladjevardi S, McGrath S, Campbell B, Lee H, Herdy JR, et al. (2015). Directly reprogrammed human neurons retain aging-associated transcriptomic signatures and reveal age-related nucleocytoplasmic defects. Cell Stem Cell 17, 705–718. [PubMed: 26456686]

Mozzetta C, Pontis J, Fritsch L, Robin P, Portoso M, Proux C, Margueron R, and Ait-Si-Ali S (2014). The histone H3 lysine 9 methyltransferases G9a and GLP regulate polycomb repressive complex 2-mediated gene silencing. Mol. Cell 53, 277–289. [PubMed: 24389103]

Muratore CR, Rice HC, Srikanth P, Callahan DG, Shin T, Benjamin LNP, Walsh DM, Selkoe DJ, and Young-Pearse TL (2014). The familial Alzheimer's disease APPV717I mutation alters APP processing and Tau expression in iPSC-derived neurons. Hum. Mol. Genet 23, 3523–3536. [PubMed: 24524897]

Park I-H, Lerou PH, Zhao R, Huo H, and Daley GQ (2008). Generation of human-induced pluripotent stem cells. Nat. Protoc 3, 1180–1186. [PubMed: 18600223]

Prince M, Comas-Herrera MA, Knapp M, Guerchet M, and Karagiannidou MM (2016). World Alzheimer Report 2016: Improving Healthcare for People Living with Dementia: Coverage, Quality and Costs Now and in the Future (Alzheimer's Disease International).

Pruszak J, Ludwig W, Blak A, Alavian K, and Isacson O (2009). CD15, CD24, and CD29 define a surface biomarker code for neural lineage differentiation of stem cells. Stem Cells 27, 2928–2940. [PubMed: 19725119]

Schoenherr CJ, and Anderson DJ (1995). The neuron-restrictive silencer factor (NRSF): a coordinate repressor of multiple neuron-specific genes. Science 267, 1360–1363. [PubMed: 7871435]

Snowdon DA, Greiner LH, and Markesbery WR (2000). Linguistic ability in early life and the neuropathology of Alzheimer's disease and cerebrovascular disease. Findings from the Nun Study. Ann. N Y Acad. Sci 903, 34–38. [PubMed: 10818486]

Sproul AA, Jacob S, Pre D, Kim SH, Nestor MW, Navarro-Sobrino M, Santa-Maria I, Zimmer M, Aubry S, Steele JW, et al. (2014). Characterization and molecular profiling of PSEN1 familial Alzheimer's disease iPSCderived neural progenitors. PLoS One 9, e84547. [PubMed: 24416243]

Tsai M-C, Manor O, Wan Y, Mosammaparast N, Wang JK, Lan F, Shi Y, Segal E, and Chang HY (2010). Long noncoding RNA as modular scaffold of histone modification complexes. Science 329, 689–693. [PubMed: 20616235]

von Schimmelmann M, Feinberg PA, Sullivan JM, Ku SM, Badimon A, Duff MK, Wang Z, Lachmann A, Dewell S, Ma'ayan A, et al. (2016). Polycomb repressive complex 2 (PRC2) silences genes responsible for neurodegeneration. Nat. Neurosci 19, 1321–1330. [PubMed: 27526204]

Winston CN, Goetzl EJ, Akers JC, Carter BS, Rockenstein EM, Galasko D, Masliah E, and Rissman RA (2016). Prediction of conversion from mild cognitive impairment to dementia with neuronally derived blood exosome protein profile. Alzheimers Dement. (Amst.) 3, 63–72. [PubMed: 27408937]

Yagi T, Ito D, Okada Y, Akamatsu W, Nihei Y, Yoshizaki T, Yamanaka S, Okano H, and Suzuki N (2011). Modeling familial Alzheimer's disease with induced pluripotent stem cells. Hum. Mol. Genet 20, 4530–4539. [PubMed: 21900357]

Yang C-P, Gilley JA, Zhang G, and Kernie SG (2011). ApoE is required for maintenance of the dentate gyrus neural progenitor pool. Development 138, 4351–4362. [PubMed: 21880781]

Yang YJ, Baltus AE, Mathew RS, Murphy EA, Evrony GD, Gonzalez DM, Wang EP, Marshall-Walker CA, Barry BJ, Murn J, et al. (2012). Microcephaly gene links trithorax and REST/NRSF to control neural stem cell proliferation and differentiation. Cell 151, 1097–1112. [PubMed: 23178126]

Yu J-T, Tan L, and Hardy J (2014). Apolipoprotein E in Alzheimer's disease: an update. Annu. Rev. Neurosci 37, 79–100. [PubMed: 24821312]

Yuan SH, Martin J, Elia J, Flippin J, Paramban RI, Hefferan MP, Vidal JG, Mu Y, Killian RL, Israel MA, et al. (2011). Cell-surface marker signatures for the isolation of neural stem cells, glia and neurons derived from human pluripotent stem cells. PLoS One 6, e17540. [PubMed: 21407814]

Zhang Y, Pak C, Han Y, Ahlenius H, Zhang Z, Chanda S, Marro S, Patzke C, Acuna C, Covy J, et al. (2013). Rapid single-step induction of functional neurons from human pluripotent stem cells. Neuron 78, 785–798. [PubMed: 23764284]

Zhu L, Zhong M, Elder GA, Sano M, Holtzman DM, Gandy S, Cardozo C, Haroutunian V, Robakis NK, and Cai D (2015). Phospholipid dysregulation contributes to ApoE4-associated cognitive deficits in Alzheimer's disease pathogenesis. Proc. Natl. Acad. Sci. USA 112, 11965–11970. [PubMed: 26372964]

Highlights

- Sporadic AD and apolipoprotein E4 (APOE4) share a common neural transcriptome
- AD and APOE4 neural progenitors exhibit altered neural differentiation
- Loss of function of REST alters transcription and differentiation in AD and APOE4
- Nuclear lamina disruption associated with AD and APOE4may impair REST function

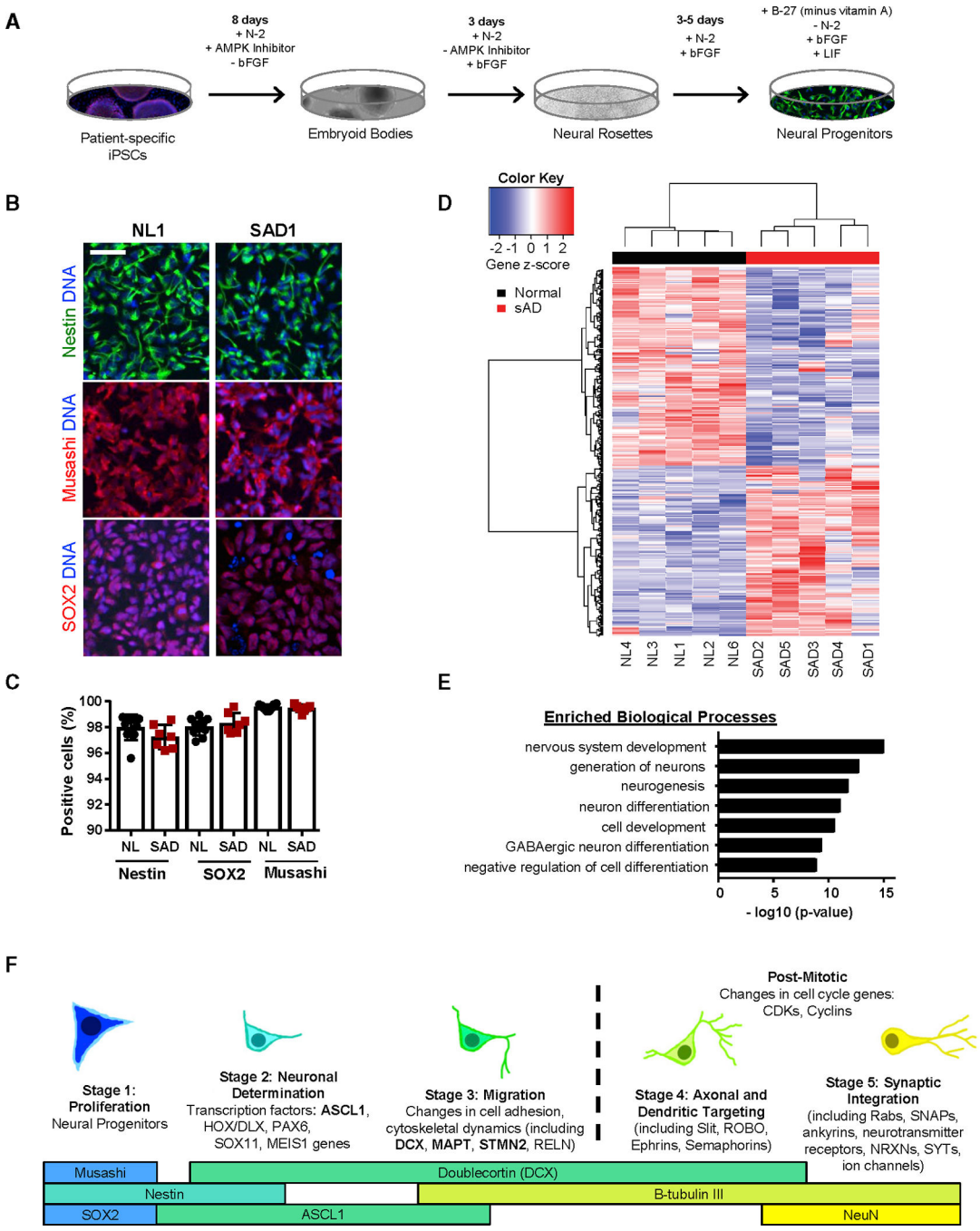

Figure 1. Differentiation and Characterization of SAD Neural Progenitors

(A) Schematic of iPSC differentiation to neural progenitor (NP) cells.

(B) Representative NP cells expressing the neural stem cell markers Nestin, Musashi, and SOX2. NL1: NP cells generated from an iPSC line derived from a normal control. SAD1: NP cells generated from an iPSC line derived from a patient with sporadic Alzheimer's disease. Scale bar, 50 mm.

(C) Quantification of neural stem cell markers Nestin, Musashi, and SOX2 shown in (B) using MetaMorph software. Data represent the mean ± SEM from 5 fields per cell line. Each point represents one cell line with 3 replicates (Table S2).

(D) Unsupervised hierarchical clustering of genes differentially expressed between sporadic Alzheimer's disease (SAD) and NL NP cells. Differentially expressedgenes (rows) and cells (columns) were clustered, and gene expression, transformed to a z-score per gene, is represented in a heatmap. NL, n = 5; SAD, n = 5.

(E) Gene Ontology (GO) biological process groups enriched in genes upregulated in SAD NP cells.

(F) Schematic of neurogenesis and neuronal differentiation based on the adult subgranular zone.

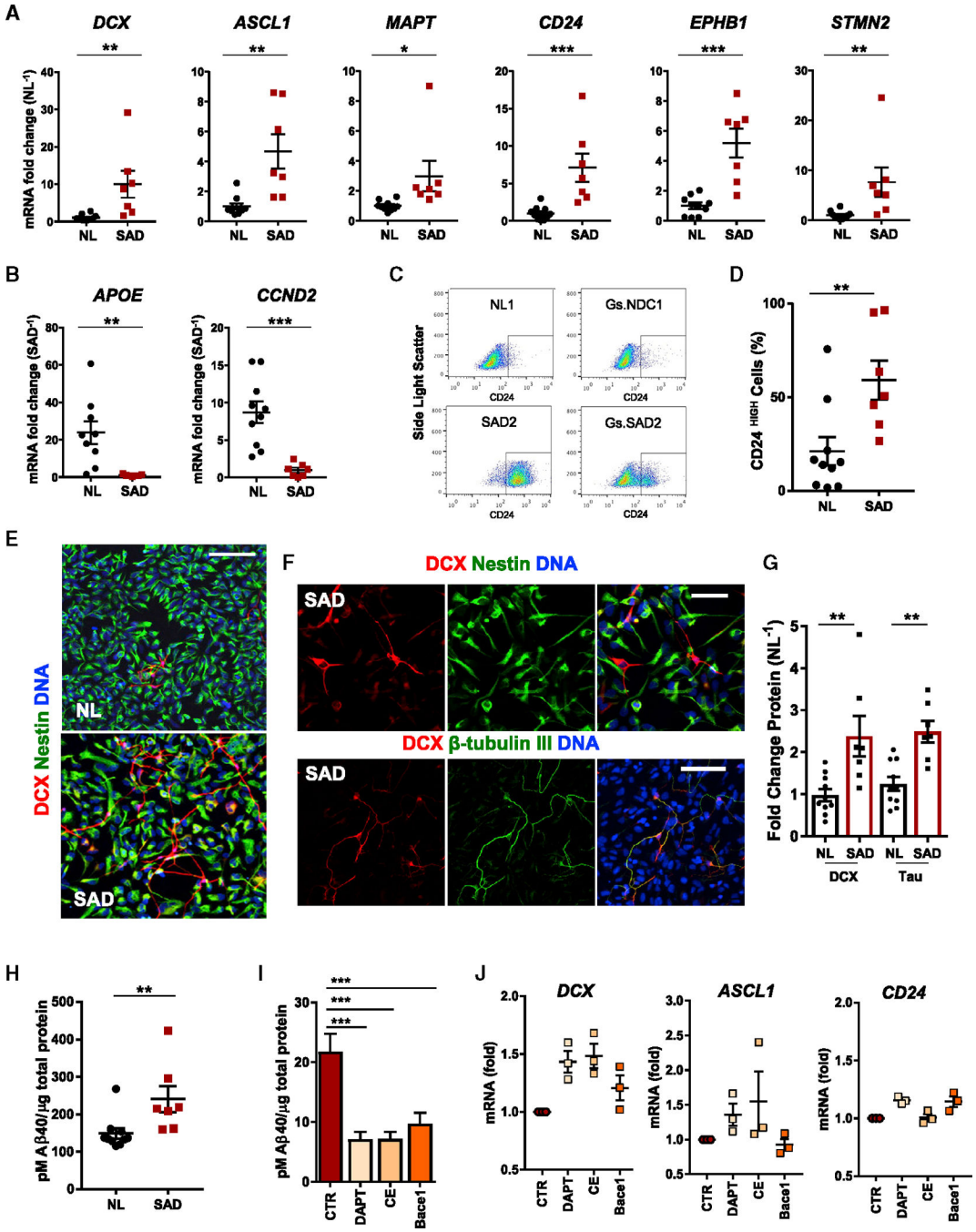

Figure 2. Accelerated Differentiation of SAD Neural Progenitors

(A) Elevated expression of neurogenesis genes in NP cells derived from SAD iPSCs. Shown is mRNA expression determined by qRT-PCR. Data represent themean fold change ± SEM relative to the mean expression level of the NL NP cell lines after normalizing to *GAPDH* expression. Each dot represents one cell line with 3 replicates (Table S2).

(B) Decreased mRNA expression of *APOE* and *CCND2* in SAD NP cells as determined by qRT-PCR. Data represent the mean ± SEM relative to the mean expression level of the SAD

lines normalized to GAPDH expression. Each dot represents one cell line with 3 replicates (Table S2).

(C) Light scatterplots from FACS analysis using the neural lineage differentiation cell surface marker CD24 in NP cells.

(D) Percentage of NP cells with high CD24 levels (inner boxed area in C) in NL and SAD NP cell lines (Table S2). Data represent the mean ± SEM; n = 3.

(E) Confocal fluorescence microscopy of representative NL3 and SAD3 NP cells after labeling for doublecortin (DCX) (red), Nestin (green), and DAPI (blue). Scalebar, 100 μm.

(F) Representative immunofluorescence image of SAD3 showing neuronal morphology in a subset of cells in SAD NP cell cultures. The top panel is double-labeledfor the NP cell marker Nestin (green) and the early neuronal marker DCX (red). The bottom panel is double-labeled for DCX (red) and another early neuronal marker b-tubulin III (green). Both panels are also labeled with DAPI (DNA, blue). Scale bar, 50 μm.

(G) Quantification of western blot analysis using DCX and tau antibodies in NL and SAD NP cells (Table S2). Protein levels were normalized to the loading controls actin and GAPDH. Data represent the mean ± SEM; n = 3..

(H) Levels of Aβ40 in 5-day conditioned cell culture medium from NL and SAD NP cells (Table S2) determined by ELISA and normalized to total protein. Values represent mean ± SEM of n = 3.

(I) Decreased Aβ40 production in SAD NP cells after treatment with the γ-secretase inhibitors DAPT (2 μM) or Compound E (CE, 20 nM), or the BACE1 inhibitor IV (0.2 μM).

(J) Fold change in mRNA expression of *DCX*, *CD24*, and *ASCL1* in SAD versus NL NP cells following inhibition of Aβ production by DAPT (2 μM) or Compound E (CE) (20 nM), or the BACE1 inhibitor IV (0.2 μM).

Values represent the mean ± SEM; n = 3 independent replications from one NL and one SAD NP cell line. *p < 0.05, **p < 0.01, and ***p < 0.001 by the MannWhitney U test.

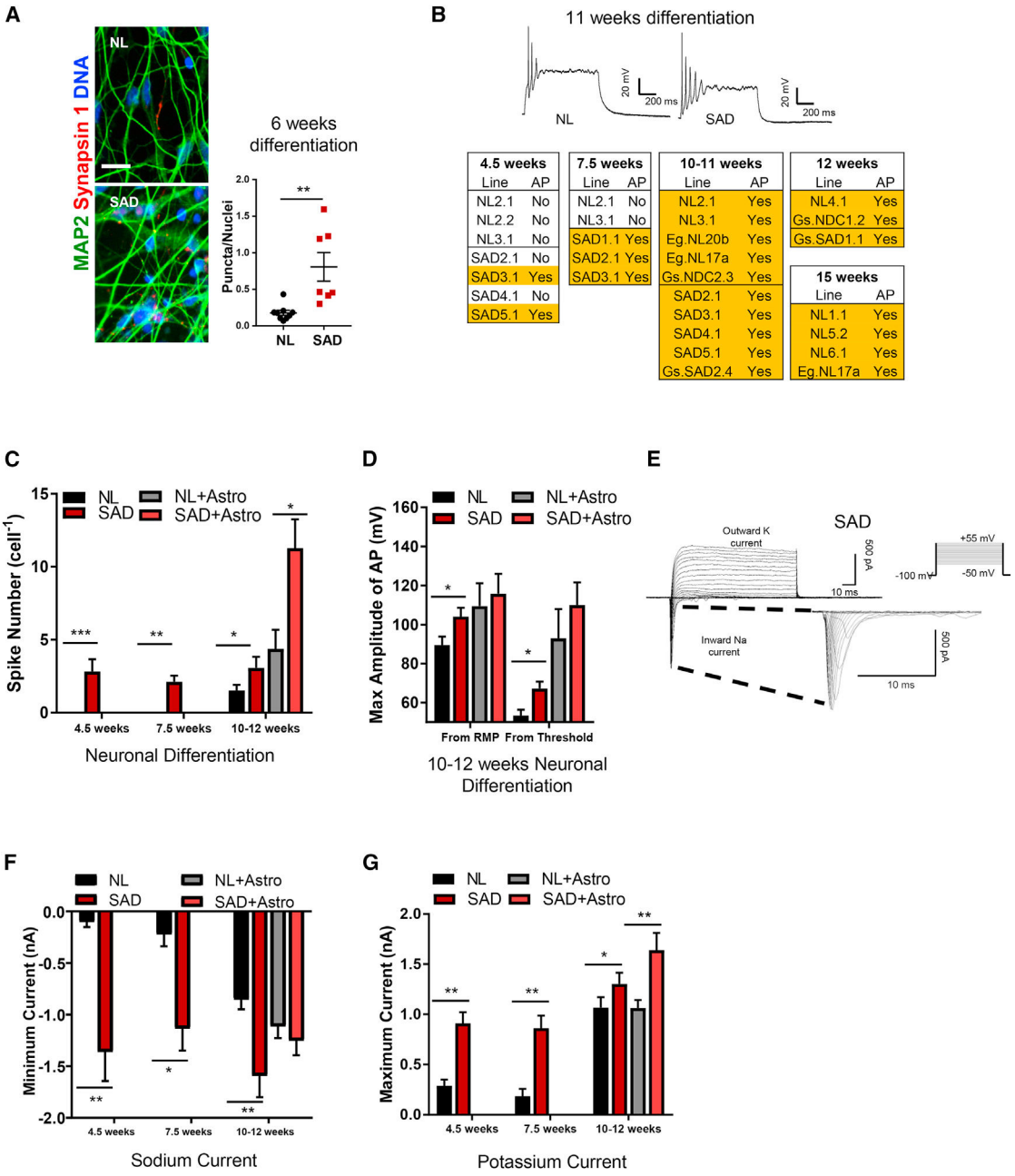

Figure 3. Accelerated Maturation and Increased Excitability of SAD Neurons.

(A) Increased synapsin-1-positive puncta in SAD neurons (days *in vitro* [DIV], 6 weeks). Representative NL4 and SAD2 neurons were labeled for synapsin 1 (red) or MAP2 (green). Data represent the mean ± SEM from 5–6 fields per cell line.

(B) Assessment of timing of action potential (AP) induction in NL and SAD neurons. Representative profiles of induced APs from SAD and NL neurons (top) andmeasured APs after 4.5–15 weeks of differentiation (bottom).

(C) AP spike number in SAD and control neurons after 4.5–12 weeks of differentiation. Some SAD and NL NP cells were co-cultured with rat astrocytes and thenassessed after 10–12 weeks of neuronal differentiation (indicated by red and gray bars).

(D) Maximum AP amplitude of NL and SAD neurons determined relative to either resting membrane potential (RMP) or threshold after 10–12 weeks ofdifferentiation.
(E) Representative current profiles following cell depolarization by voltage steps from −50 to +55 mV.
(F and G) Minimum inward (Sodium Current) (F) and maximum outward (Potassium Current) (G) currents were measured in NL and SAD neurons after the indicated duration of differentiation.
(C–G) n = 4–43 neurons; p values: *p < 0.05, **p < 0.01, and ***p < 0.001 by the Mann-Whitney U test except for (D) (Student's t test). Refer to Table S2 for experimental details.

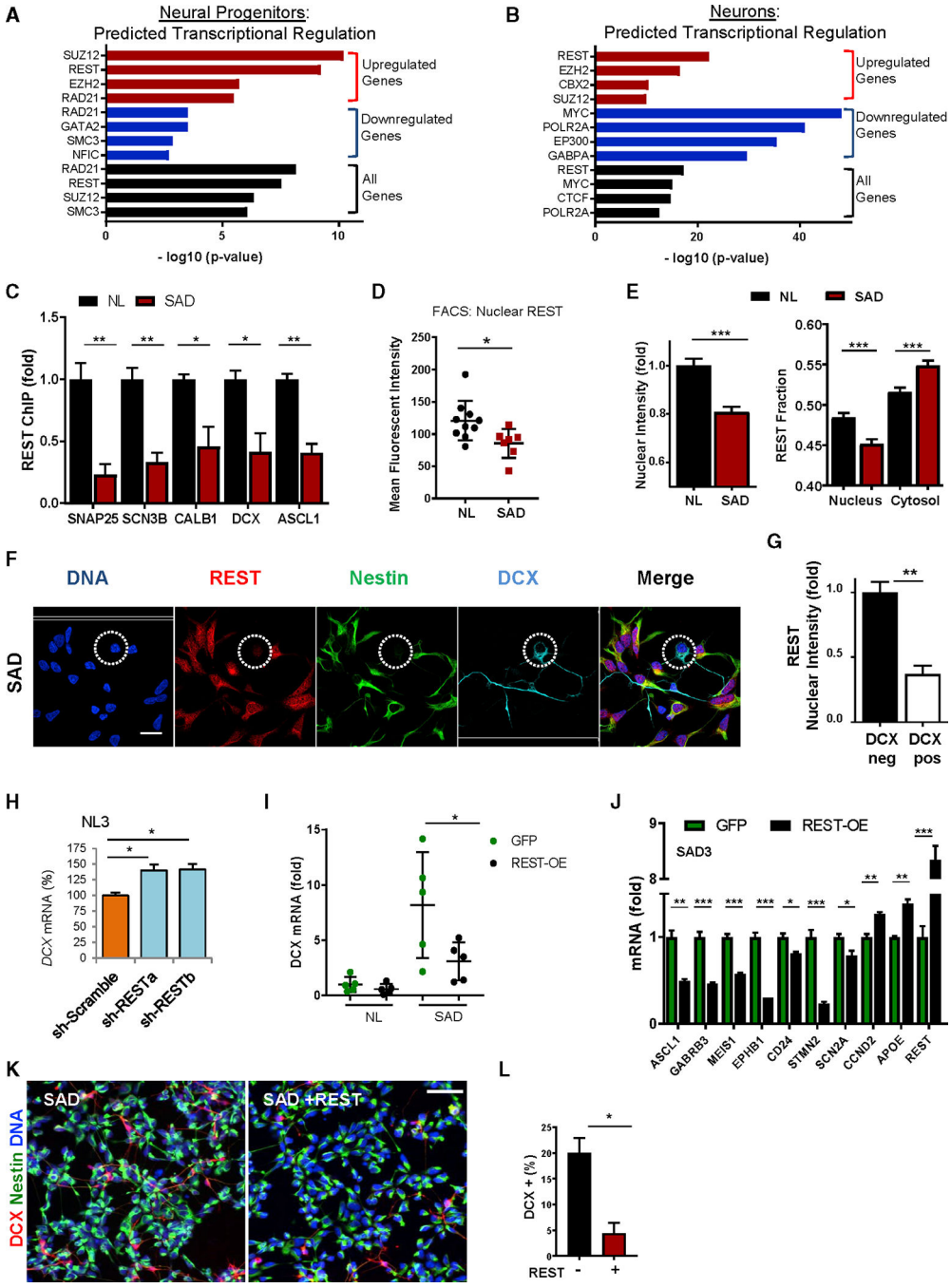

Figure 4. Altered Regulation of REST and Accelerated Neuronal Differentiation in SAD NP Cells

(A and B) Transcription factor prediction based on enrichment in genes that are differentially expressed in SAD versus NL NP cells (A) and neurons (B) using the ENCODE ChIP-seq database. Predictions are stratified for genes that were upregulated or downregulated, and all genes in the SAD versus NL comparison.

(C) REST-RE1 site binding is markedly reduced in SAD NP cells. REST ChIP-PCR (REST antibody; Millipore; #17–641) was performed for RE1 sites in *SNAP25*, *SCN3B*, *CALB1*, *DCX*, and *ASCL1*. N = 2 biological replicates per line for 10 NL and 7 SAD NP cell lines.

(D) FACS analysis and quantification of nuclear REST levels in NL and SAD NP cells. Data represent the mean ± SEM from 3–5 replicates per line for 10 NL and 7 SAD NP cell lines.
(E) Quantification of REST nuclear intensity (left) and fraction of total cellular REST signal in the nucleus (right) by confocal immunolabeling of REST (anti-REST;Millipore; #07–579). Data represent the mean ± SEM from 4 replicates in 3 SAD and 3 control NP cell lines.
(F) Immunolabeling of representative SAD4 NP cells for REST (Millipore; #07–579), nestin, and DCX. The DCX-positive soma is delineated by a dotted circle. Scalebar, 50 μm.
(G) Quantification of REST nuclear intensity in DCX-positive and DCX-negative cells. Data represent the mean ± SEM from 3 SAD NP cell lines.
(H) REST knockdown by two previously described REST shRNAs (sh-RESTa and sh-RESTb; Lu et al., 2014) increases DCX mRNA levels in the control NP cell line NL3. DCX expression levels were normalized to expression in the control shRNA-treated culture (sh-Scramble). Values represent the mean ± SEM from 3 experiments.
(I) Quantification of DCX mRNA expression in NL and SAD NP cell lines after overexpression of REST. Cells were transduced with lentiviral vectors encoding GFP (Control) or REST (REST-OE) and analyzed by qRT-PCR. Data represent fold change relative to the mean of the DCX mRNA levels in the NL lines transduced with the GFP control lentivirus and normalized to *GAPDH*. Values represent the mean ± SEM from 3 experiments.
(J) Quantification of gene expression in SAD NP cells after overexpression of REST. Cells were transduced with lentiviral vectors encoding GFP (GFP) or REST(REST-OE) and analyzed by qRT-PCR. Data represent the mean from 3 experiments ± SEM.
(K) Representative confocal immunofluorescence images of DCX-positive neuronal cells and nestin (green) in SAD3 NP cell cultures transduced with RESTlentivirus (SAD+REST) or GFP control lentiviral particles (SAD). Scale bar, 50 μm.
(L) Quantification of DCX-positive cells in the presence (+) or absence () of REST overexpression.
Data represent the mean ± SEM from four experiments. *$p < 0.05$, **$p < 0.01$, and ***$p < 0.001$ by Student's t test.

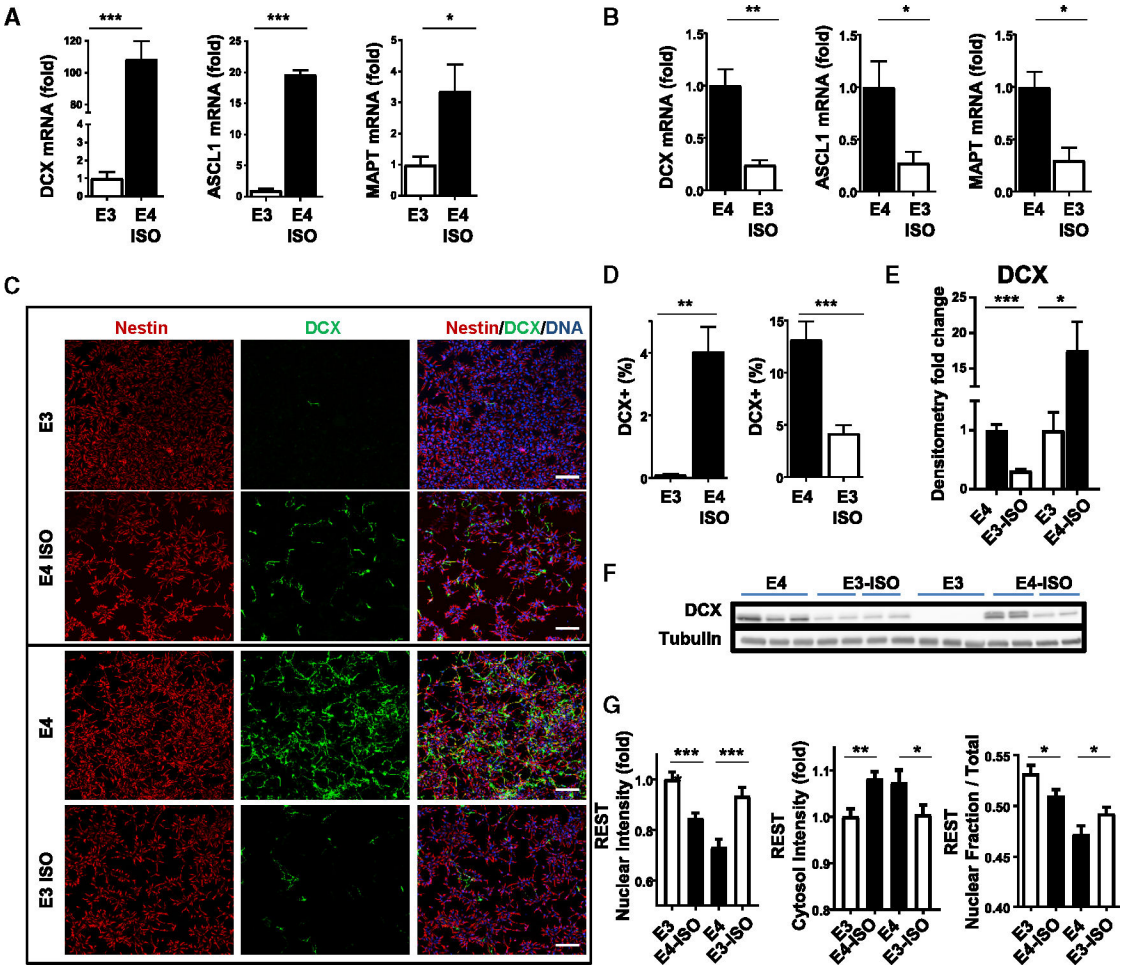

Figure 5. Altered Regulation of REST and Accelerated Neuronal Differentiation in Gene-Edited NP Cells Expressing APOE4

(A) Expression of *DCX*, *ASCL1*, and *MAPT* in APOE4 isogenic (E4 ISO) versus parental APOE3 (E3) NP cells. Data represent the mean ± SEM from 3 biological replicates of 1 APOE3 parental line and 2 individual APOE4 isogenic clones. Expression was determined by droplet digital PCR (ddPCR) and normalized to *TBP*. Isogenic lines were derived by gene editing from the APOE3/E3 and APOE4/E4 lines AG09173 and AG10788, respectively (see Table S1).

(B) Expression of *DCX*, *ASCL1*, and *MAPT* in APOE4 parental (E4) versus isogenic APOE3 (E3 ISO) NP cells. Data represent the mean ± SEM from 3 biological replicates of 1 APOE4 parental line and 2 individual APOE3 isogenic clones, and was normalized to *TBP*.

(C) Immunolabeling for nestin (red) and DCX (green) in isogenic APOE NP cells. Shown are E3 parental NP cells (E3), E4 isogenic NP cells (E4 ISO), E4 parental NPcells (E4), and E3 isogenic NP cells (E3-ISO). Scale bar, 100 μm.

(D) Quantification of the immunolabeling shows a marked increase in DCX-positive cells in both parental APOE4 and isogenic APOE4 cell lines relative to APOE3. Data represent the mean ± SEM from 5 fields from 3 independent biological replicates.

(E and F) Quantification (E) of western blot analysis (F) of DCX protein levels in 2 E3-ISO lines compared to parental E4 and 2 E4-ISO lines compared to E3.

(G) Individual cell analysis of REST in the nucleus and cytosol, as well as the fraction of total cellular REST in the nucleus (Nuclear Fraction/Total) after REST immunolabeling (REST Antibody; Millipore; #07–579). *$p < 0.05$, **$p < 0.01$ and ***$p < 0.001$ by Student's t test.

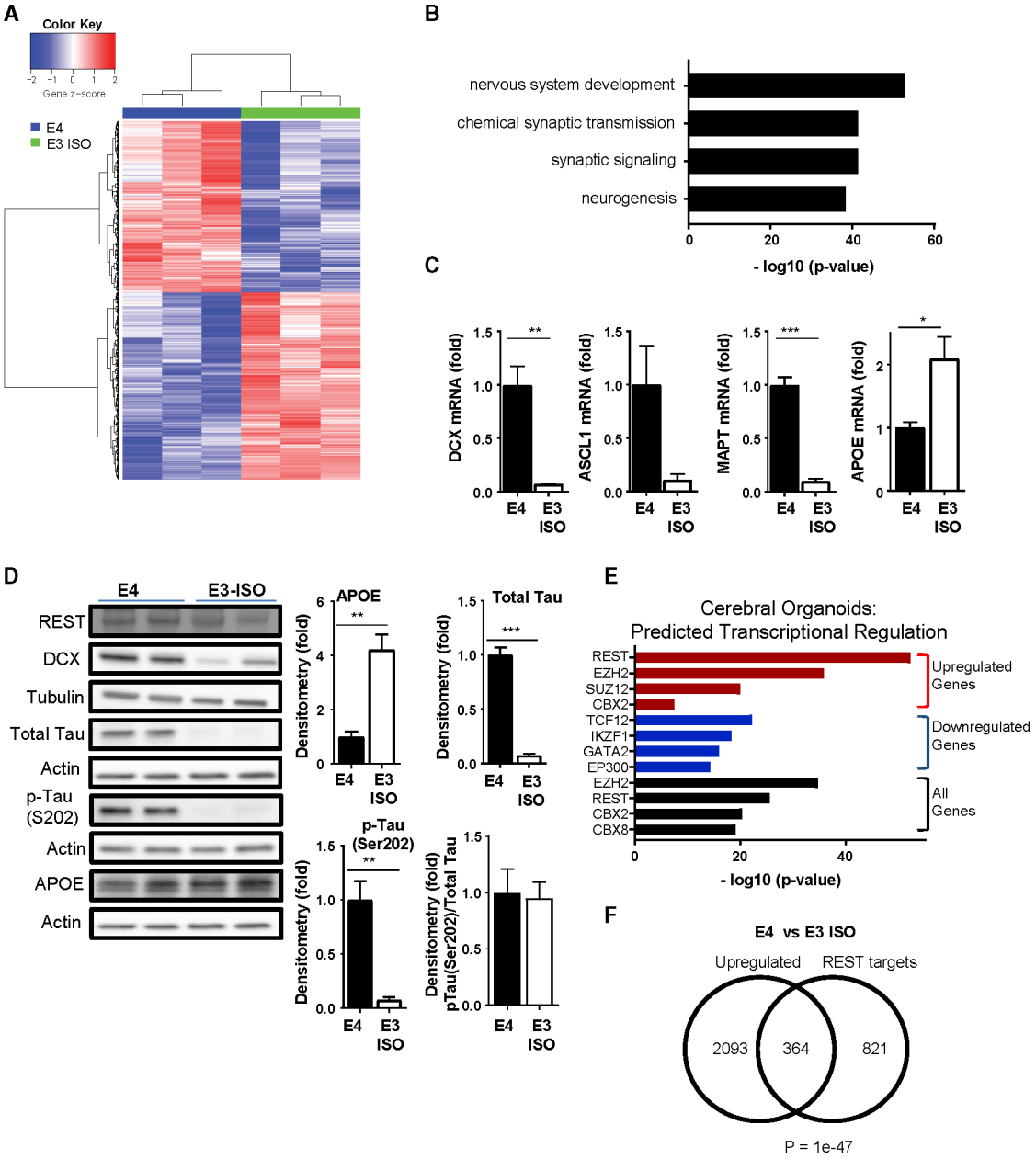

Figure 6. Altered Gene Regulation and Neuronal Differentiation in APOE4 Cerebral Organoids

(A) Unsupervised hierarchical clustering of genes differentially expressed between parental APOE4 and isogenic APOE3 cerebral organoids after 46 days of maturation. Differentially expressed genes (rows) and organoids (columns) were clustered, and gene expression was transformed to a z-score and represented in the heatmap. Parental APOE4 (E4), n = 3; isogenic APOE3 (E3 ISO), n = 3.

(B) GO biological process groups enriched in genes upregulated in parental APOE4 compared to isogenic APOE3 organoids.

(C) Expression of *DCX*, *ASCL1*, *MAPT* and *APOE* mRNA in parental APOE4 (E4) versus isogenic APOE3 (E3 ISO) organoids. Data represent the mean ± SEM from 3 experiments using a total of 45 individual organoids (DIV, 46 days).

(D) Western blot analysis of REST (Millipore; #07–579), DCX, total tau (Tau5), p-tau(Ser202), and APOE in parental APOE4 and isogenic APOE3 organoids. Eachlane was loaded with protein lysate from 3 organoids (left). Normalization to tubulin or actin shown in adjacent western blots was used for quantification (right). Data represent the mean ± SEM from 3 individual lysates.

(E) Transcription factor prediction based on enrichment in APOE4 differentially expressed genes using the ENCODE ChIP-seq database. Predictions are stratifiedfor genes that were upregulated or downregulated, and all genes in the APOE4 versus APOE3 comparison.

(F) Venn diagram illustrating the overlap of APOE4-upregulated genes and REST targets based on RE1 motif analysis (see STAR Methods).

Overlap significance was determined by Fisher's exact test. For (C) and (D): *$p < 0.05$, **$p < 0.01$, and ***$p < 0.001$ by unpaired Student's t test.

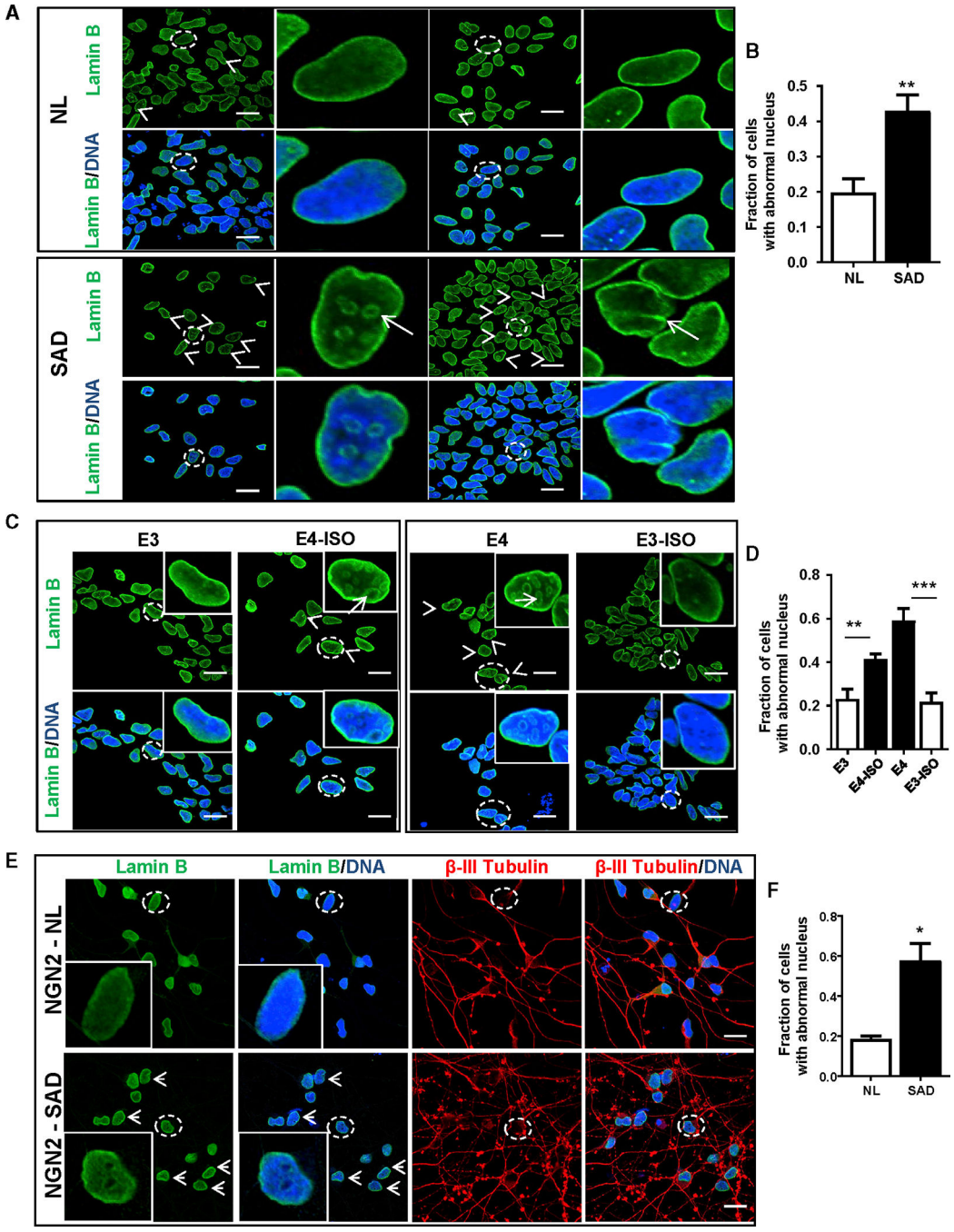

Figure 7. Disruption of the Nuclear Lamina in SAD and APOE4 NP Cells

(A) Representative confocal immunofluorescence microscopy of NL1 and SAD4 NP cell lines for lamin B. Dotted circles delineate nuclei represented in the highermagnification images. Arrowheads indicate nuclei with abnormal morphology. Scale bar, 50 μm.

(B) Quantification of cells showing abnormal nuclear lamina morphology. Data represent the mean ± SEM from 3 biological replicates using 3 different NL and SAD NP cell lines.

(C) Representative images from APOE isogenic NP cell lines after lamin B immunolabeling. Scale bar, 50 μm.

(D) Quantification of cells with abnormal nuclear morphology. Data represent the mean ± SEM from 3 biological replicates using 2 different isogenic lines.
(E) Representative images from NL3 and SAD2 neurons differentiated by doxycycline induced NGN2 overexpression after lamin B immunolabeling (neurons DIV,13 days). Scale bar, 50 μm.
(F) Quantification of cells with abnormal nuclear morphology.
Data represent the mean ± SEM from 3 NL and 4 SAD lines; *$p < 0.05$, **$p < 0.01$ and ***$p < 0.001$ by unpaired Student's t test.

KEY RESOURCES TABLE

REAGENT or RESOURCE	SOURCE	IDENTIFIER
Antibodies		
Oct-3/4 (H-134) antibody	Santa Cruz Biotechnology	Cat# sc-9081; RRID:AB_2167703
Anti-TRA-1–81, clone TRA-1–81 antibody	Millipore	Cat# MAB4381; RRID:AB_177638
Nanog (H-155) antibody	Santa Cruz Biotechnology	Cat# sc-33759; RRID:AB_2150401
Anti-Sox2 antibody	Millipore	Cat# AB5603; RRID:AB_2286686
Anti-SOX-2 Monoclonal Antibody	Millipore	Cat# MAB4343; RRID:AB_827493
Anti-Nestin, clone 10C2 antibody	Millipore	Cat# MAB5326; RRID:AB_11211837
Anti-Musashi-1 antibody	Millipore	Cat# AB5977; RRID:AB_92184
MAPK1/MAPK3 (phospho T202/204) monoclonal antibody, clone G15-B	Abnova Corporation	Cat# MAB1637; RRID:AB_1707889
Rabbit Anti-Neuronal Class III beta-Tubulin Purified Monoclonal Antibody, Unconjugated, Clone TUJ1	Covance Research Products Inc	Cat# MRB-435P-100; RRID:AB_663339
Doublecortin Antibody	Cell Signaling Technology	Cat# 4604S; RRID:AB_10693771
Doublecortin (C-18) antibody	Santa Cruz Biotechnology	Cat# sc-8066; RRID:AB_2088494
VGLUT1 mouse monoclonal antibody	MediMABS	MM-0016-P
Anti-GABA antibody produced in rabbit	Sigma-Aldrich	Cat# A2052; RRID:AB_477652
Anti-Synapsin I Rabbit pAb antibody	Millipore	Cat# 574777; RRID:AB_2200124
Anti-MAP2, clone AP20 antibody	Millipore	Cat# MAB3418; RRID:AB_94856
Anti-Actin Monoclonal Antibody, Unconjugated, Clone AC-40	Sigma-Aldrich	Cat# A3853; RRID:AB_262137
Anti-REST antibody	Millipore	Cat# 07–579; RRID:AB_11211936
Tau Monoclonal Antibody (TAU-5)	Thermo Fisher Scientific	Cat# AHB0042; RRID:AB_2536235
Mouse Anti-alpha-Tubulin Monoclonal Antibody, Unconjugated, Clone B-5-1-2	Sigma-Aldrich	Cat# T6074; RRID:AB_477582
Non-phospho (Active) β-Catenin (Ser45) (D2U8Y) XP® Rabbit mAb antibody	Cell Signaling Technology	Cat# 19807; RRID:AB_2650576
Cleaved Notch1 (Val1744) (D3B8) Rabbit mAb antibody	Cell Signaling Technology	Cat# 4147S; RRID:AB_2153348
Notch1 (D6F11) XP Rabbit mAb antibody	Cell Signaling Technology	Cat# 4380, RRID:AB_10691684
Phospho-Tau (Thr231) Monoclonal Antibody (AT180)	Thermo Fisher Scientific	Cat# MN1040; RRID:AB_223649
Mouse Anti-Phospho-PHF-tau pSer202/ Thr205 Monoclonal Antibody, Clone AT8	Thermo Fisher Scientific	Cat# MN1020; RRID:AB_223647
Goat Anti-Lamin B (M-20)	Santa Cruz Biotechnology	Cat# sc-6217; RRID:AB_648158
Critical Commercial Assays		
Human βAmyloid(1–40) ELISA Kit Wako	Wako	292–62301
Amyloid beta 42 Human ELISA Kit	Invitrogen	KHB3441
Amyloid beta 40 Human ELISA Kit	Invitrogen	KHB3481
Deposited Data		
Neuron, NPC, iPSC Microarray	This paper	GEO: GSE117589
Cerebral organoid RNA-seq	This paper	GEO: GSE117589
Experimental Models: Cell Lines		

REAGENT or RESOURCE	SOURCE	IDENTIFIER
Human Fibroblasts	Coriell	AG04455
Human Fibroblasts	Coriell	AG08125
Human Fibroblasts	Coriell	AG08379
Human Fibroblasts	Coriell	AG08509
Human Fibroblasts	Coriell	AG14244
Human Fibroblasts	Coriell	AG09173
Human Fibroblasts	Coriell	AG06869
Human Fibroblasts	Coriell	AG07376
Human Fibroblasts	Coriell	AG21158
Human Fibroblasts	Coriell	AG08243
Human Fibroblasts	Coriell	AG10788
Human iPSC	Boulting et al., 2011	Eg.NL17a
Human iPSC	Boulting et al., 2011	Eg.NL20b
Human iPSC	Israel et al., 2012	Gs.NDC1
Human iPSC	Israel et al., 2012	Gs.NDC2
Human iPSC	Israel et al., 2012	Gs.SAD1
Human iPSC	Israel et al., 2012	Gs.SAD2
qPCR primers for *GAPDH, β-Actin, DCX, STM2, CD24, EPHB1, ASCL1, MAPT, APOE, CCND2, ROBO2, RAB3C, STXBP5, SCN2A, KCNMA1, SPON1, COL11A1, HOXA2, ZIC3, MEIS1, REST, EPHB1, GABRB3-RE1, DCX-RE1* see Table S7	This paper	N/A
ddPCR probes for *TBP, GDAP1L1, DLG4, REST, ASCL1, MAPT, NANOG, PAX6, RBFOX3, SYP, GFAP* see Table S7	Bio-Rad	See Table S7
Recombinant DNA		
pMIG-hKLF4	Addgene	#17227
pMIG-hSOX2	Addgene	#17226
MSCV hc-MYC	Addgene	#18119
pMIG-hOCT4	Addgene	#17225
pMD2.G	Addgene	#12259
FUGW-GFP	Addgene	#14883
FUGW-hREST	Lu et al., 2014	N/A
REST-shRNA 1	Lu et al., 2014	N/A
REST-shRNA 2	Lu et al., 2014	N/A
Software and Algorithms		
STAR	PMID 23104886	version 2.5.4a
edgeR	PMID 19910308	version 3.20.9
limma	PMID 25605792	version 3.34.9
FIMO	PMID 21330290	version 4.10.1
TopGO	Alexa and Rahnenfuhrer, 2016; https://bioconductor.org/packages/release/bioc/html/topGO.html	version 2.32.0

REAGENT or RESOURCE	SOURCE	IDENTIFIER
SuperExactTest	PMID 26603754	version 1.0.0
Gene annotation, Gene Ontology	Ensembl BioMart	GRCh38.p12 Accessed on March 4, 2018
Custom Affymetrix CDF	PMID 16284200	HGU133Plus2_Hs_ENSG version 22.0.0
Enrichr ENCODE_TF_ChIP-seq_2015 database	PMID 23586463	Accessed on March 8, 2018